

CHANNEL MODELS FOR TERRESTRIAL WIRELESS COMMUNICATIONS: A SURVEY (*)

PAOLO BARSOCCHI, NATIONAL RESEARCH COUNCIL – ISTI INSTITUTE

ABSTRACT

The demand for wireless communications systems is ever increasing in all the human- life activities. Anyway, the high diffusion rate of this technology provoked some confusion in the user, as the industry developed many different wireless systems and services, which often were not able to interact each other. A WLAN (wireless local area network) is a local area network (LAN) that uses high-frequency radio links instead of terrestrial wires to communicate among nodes. It allows mobile users to connect to a LAN through a wireless radio frequency (RF) connection. This technology provides connectivity also where wiring is impossible or costly. Wireless technology can range from WLANs and cellular networks to headphones and microphones connections. It includes infrared (IR) devices, such as remote controls, cordless keyboards, and mice, all of which have a transmitter and a receiver.

The aim of this tutorial is to introduce readers to wireless channel models, by providing a selection of the most popular ones. The types of fading typical of the wireless environment are also presented, together with the relevant propagation models. The author is currently carrying out vast indoor and outdoor measurement campaigns at the packet level, in order to define channel models derived from the measures collected. A few preliminary results of this activity are also presented.

Wireless networks have become increasingly popular due to their ease deployment and low cost, compared to wired networks. The mobile radio channel places strong limitations on the performance of wireless communication systems because the transmission principles in wireless communications are dramatically more complex than those of wired networks. The transmission path between the transmitter and the receiver can vary from a simple line of sight (LOS) to a line that is severely obstructed by buildings, mountains, or foliage. Unlike wired channels, whose characteristics are stationary and predictable, radio channels performance is extremely variable and not treatable with a simple analysis. Modelling a radio channel has been one of the most difficult parts in the mobile radio system design, and it is based on measurements specifically made for an intended communication system. Propagation models are the base for channel modelling, as they try to describe the way a radio signal changes during its travel from the transmitter to the receiver. Propagation models have traditionally focused on predicting the average signal strength at the receiver, set at a given distance from the transmitter, as well as the variability of the signal strength in close spatial proximity of a particular location. Propagation models that predict the mean signal strength for an arbitrary transmitter-receiver (T-R) separation distance are useful to estimating the radio coverage area of a transmitter; they are called *large-scale* propagation models, since they characterize the average signal strength over long time spans and large T-R separation distances (several hundred meters). Propagation models that characterize the rapid fluctuations of the

(*) Work funded by the Italian Ministry of University and Research (MIUR) in the framework of the *IS-MANET* project and by the European Commission in the framework of the *SatNEx NoE project* (contract N. 507052).

receiver signal strength over very short travel distances (few wavelengths) or short time durations (in the order of seconds) are called *small-scale* or *fading* models.

Many research activities, such as simulation and system design, need a model of the channel under study. Models are available in the literature, but often it is difficult to match the real scenario to the theoretical models at disposal. The aim of this tutorial is to analyse the behaviour of a wireless channel at the physical level, and to present the relative channel models. A good knowledge of the physical layer and the fundamental limitations in the performance of mobile communication systems are necessary tools for engineers, as well as for research scientists who wish to develop new channel models.

The tutorial is organized as follows. Section I describes a typical scenario for terrestrial mobile radio channels and the principal causes of information loss (*multipath fading*). Conditions that cause multipath fading are also described, i.e. the fading effects that characterize mobile communications. The knowledge of the properties of the time-varying frequency and space-dispersive mobile radio channel is necessary for a good understanding of the phenomena that occur in wireless communications and for the design of mobile communication systems and networks. Section II presents the propagation models that characterize signal strength over large transmitter-receiver separation distances (large-scale propagations models); models that characterize the rapid fluctuations of the received signal strength over short distances (small-scale models) are illustrated in Section III. Section IV contains some considerations regarding the outgoing research work in wireless channel modelling carried on by the author. Conclusions are drawn in Section V. An Appendix, which contains some basic concepts in wireless communications is also provided for reader's convenience. The numeration used in the references follows the Section the indicated paper refers to. As an example, [x.y] indicates the reference y used in Section x.

Far away from being exhaustive, this tutorial aims at providing the bases for further studies of this complex research argument.

I. The terrestrial wireless multi-path fading channel

1.1 The environment

In cellular communication systems the service area is divided into *cells*, each covered by a *base station*. If a multiplicity of base stations share the same frequency channel to send data towards their mobile users (*forward links*), each communication between a base station and a particular user will also reach all other users in the form of co-channel interference [1.1, 1.2]. However, the greater the distance between the mobile and the interfering transmitter, the weaker the interference becomes, due to propagation loss. To ensure a good quality of the service, the signal received in a cell must be strong. Once the signal has crossed the boundary of a cell, it becomes *interference*; thus, it is necessary that it is as weak as possible. Since this is difficult to obtain, the channel frequency is usually not reused in adjacent cells. If reused, the co-channel interference may damage the signal reception in the adjacent cells, and the quality of the service may severely degrade [1.3 - 1.6]. The same principle applies in the *return link* (from the mobile towards the base station). The difference in the received signal strength between the nearest and the farthest mobile user in a given cell can be in the range of 100 dB, which can cause saturation at the receivers of the weakest signal or an excessive amount of adjacent channel interferences [1.7]. In order to avoid such a problem, the transmitted power at the base station should be set inversely proportional to the *effective distance* of the mobile from the base station; *effective distance* includes effects such as shadowing or deep fading, both of which increase the effective distance [1.8].

In wireless mobile communications, the electromagnetic waves often do not directly reach the receiver due to obstacles that block the line of sight path. A signal travels from transmitter to receiver over a multiple-reflection path; this phenomenon is called *multipath propagation* and

causes fluctuations in the receiver signal's amplitude and phase. The sum of the signals can be constructive or destructive. A typical scenario of mobile radio communications is shown in Fig. 1, where the three main mechanisms that impact the signal propagation are depicted [1.9].

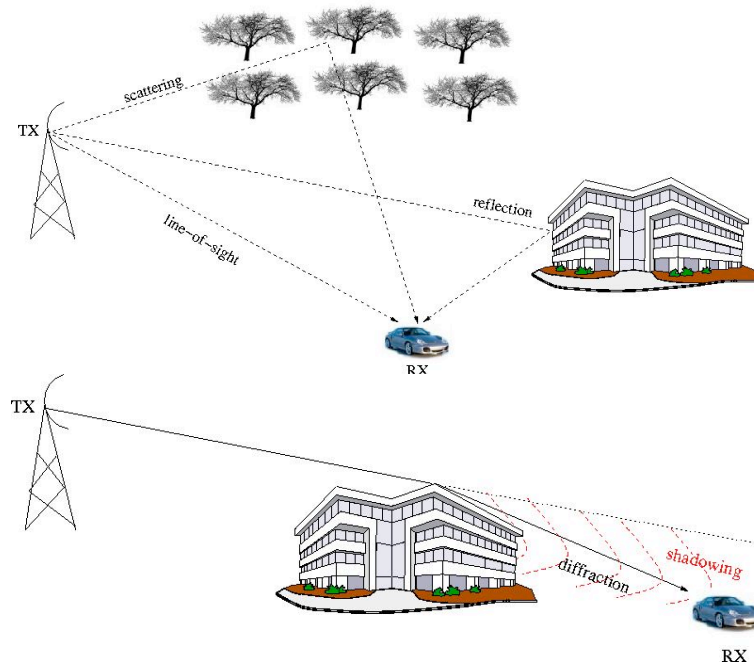


Fig. 1. A typical scenario of mobile radio communications

Those mechanisms are:

- *Reflection*. It occurs when the electromagnetic wave bumps against a smooth surface, whose dimensions are large compared with the signal wavelength.
- *Diffraction*. When a building whose dimensions are larger than the signal wavelength obstructs a path between transmitter and receiver, new secondary waves are generated. This phenomenon is often called *shadowing*, because the diffracted field can reach the receiver even when shadowed by an impenetrable obstruction (no line of sight).
- *Scattering*. It happens when a radio wave bumps against a rough surface whose dimensions are equal to or smaller than the signal wavelength. In the urban area, typical obstacles that cause scattering are lampposts, street signs, and foliage.

Another negative influence on the characteristics of the radio channels is the *Doppler effect*, due to the motion of the mobile station. The Doppler effect causes a frequency shift of each portion of transmitted waves [1.10]. Relation (1.1) gives the Doppler frequency of the incident wave:

$$f = f_{\max} \cos \alpha, \quad (1)$$

where

$$f_{\max} = \frac{v}{c_0} f_0 \quad (2)$$

is the maximum Doppler frequency or shift, which depends on the ratio of the speed of the vehicle (v), the speed of the light (c_0), and the carried frequency (f_0); α is the angle of arrival of the incident wave (Fig. 2) with respect to the mobile velocity vector [1.11, 1.12].

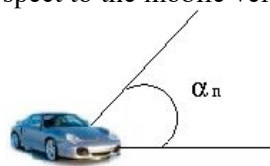


Fig. 2. Angle of arrival of the n -th incident wave

1.2 Fading types

Reflection, diffraction, and scattering have a great impact on the signal power, and they constitute the main reasons for signal attenuation (*fading*). The interaction between the waves derived by reflection, diffraction and scattering cause multipath fading at a specific location. Fading can be categorized into two main types: *large-scale fading* and *small-scale fading* [1.13 – 1.15]. *Large-scale fading* is due to motion in a large area, and can be characterized by the distance between transmitter and receiver. *Small-scale fading* is due to small changes in position (as small as half wavelength) or to changes in the environment (surrounding objects, people crossing the line of sight between transmitter and receiver, opening or closing of doors, etc.). Figure 3 illustrates the wireless channel fading types.

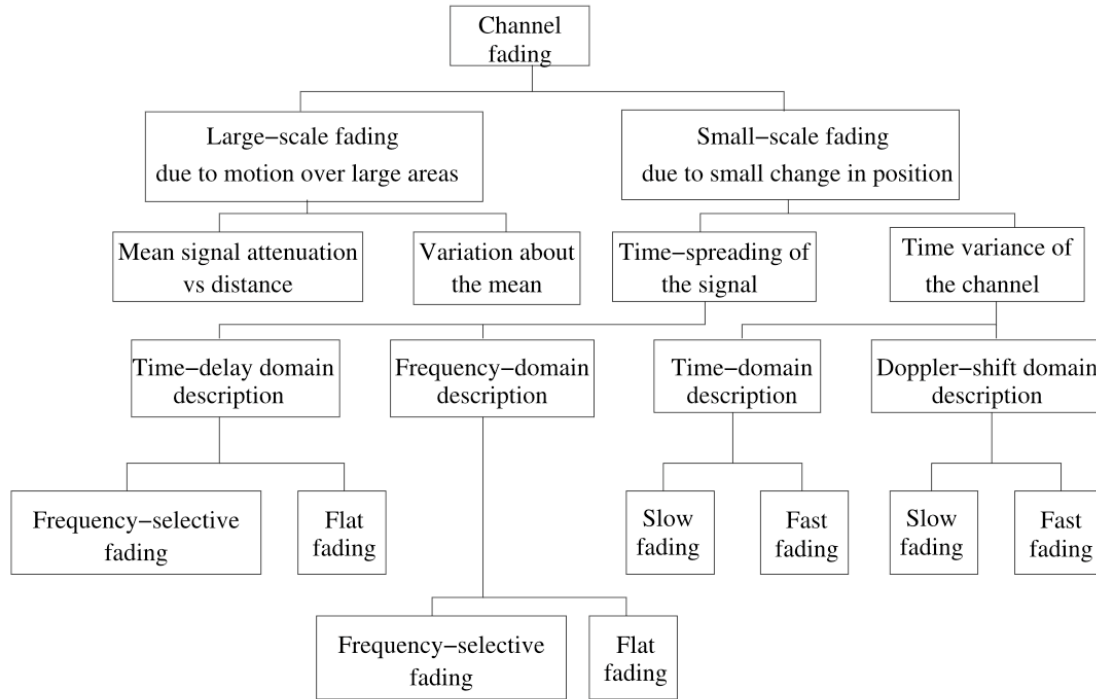


Fig. 3. Channel fading types⁽¹⁾

In order to outline the main differences between large-scale and small-scale fading, let us consider a received signal, which is represented by the convolution between the transmitted signal $s(t)$ and the impulse response function of the channel $h_c(t)$:

$$r(t) = s(t) \otimes h_c(t) \quad (3)$$

The received signal can be seen as the product of two random variables [1.16]

$$r(t) = m(t) \cdot r_0(t) \quad (4)$$

where $m(t)$ is the *large-scale fading component*, and $r_0(t)$ the *small-scale fading component*.

$m(t)$ is the *local mean* of the received signal, usually characterised by a *lognormal probability density function*, which means that the magnitude, measured in decibel, has a Gaussian probability density function. $r_0(t)$ is sometimes referred to as a *multipath fading*. Figure 4 highlights these two effects.

⁽¹⁾ Figure extracted from reference [2.6]

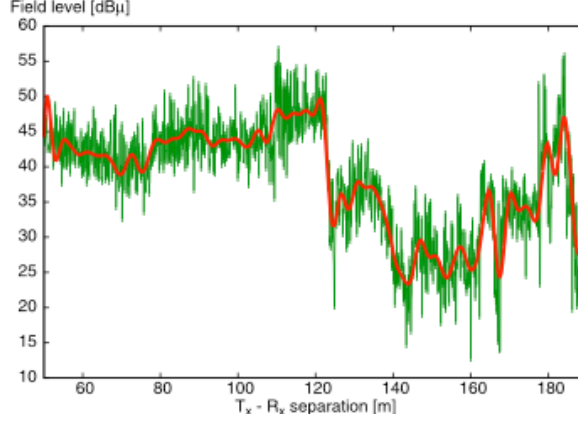


Fig. 4. Small-scale fading (green line) and large-scale fading (red line) versus the transmitter receiver separation distance

II. The terrestrial wireless large-scale propagation models

Large-scale fading propagation models are used at the physical layer to predict the mean signal strength for an arbitrary transmitter-receiver (T-R) separation distance. The *free-space* propagation model and the *lognormal* one are two generic propagation models that are often used as a basis for specific models [2.1], as we will see in next sub-sections.

The *free-space propagation model* is an ideal model used to compute the received signal strength when there is a direct LOS between a transmitter and a receiver unit, placed at distance d between them, without any obstacles near the line of sight. The power received in free space (P_r) is given by the Friis transmission equation

$$P_r(d) = \frac{P_t G_t G_r \lambda^2}{(4\pi)^2 d^2 L}, \quad (5)$$

where P_t is the transmitted power, G_t is the transmitter antenna's gain, G_r is the receiver antenna's gain, λ is the wavelength (expressed in the same unit as d), L is the system loss factor (≥ 1 , for example filter losses, antenna losses, etc...). From now on, without loss in generality, we assume $L=1$. The path loss or *free-space loss* L_{fs} is defined as the ratio between the effective transmitted power and the received power, which includes the effects of the antenna gains [2.2].

$$L_{fs}|_{dB} = 10 \log \left(\frac{P_t G_t G_r}{P_r L} \right) = 20 \log \left(\frac{4\pi d}{\lambda} \right) \quad (6)$$

The antenna gain is given by

$$G = \frac{4\pi A_e}{\lambda^2} \quad (7)$$

where A_e is the effective size of the antenna.

Theoretical and measurement-based models, developed in generic environments with or without LOS, indicate that the average received signal power decreases with the distance raised to some exponent [2.3]. In (5) the exponent is 2, that is, the received power decreases as the square of distance. In the *lognormal path loss propagation model* the average path loss for an arbitrary T-R couple, $\bar{L}_p(d)$, is expressed as a function of the distance d by using a *path loss exponent*, independently of the presence of a direct LOS between the transmitter and the receiver units.

$$\bar{L}_p(d) \propto \left(\frac{d}{d_0} \right)^n, \quad (8)$$

where n is the path loss exponent that indicates the rate at which the path loss increases with the distance, and d_0 is called the *free-space close-in reference distance* [2.3]. The selected value of

d_0 must be appropriate for the propagation environment. In large cellular systems, 1 km and 1 mile are commonly used as reference distances, whereas in microcellular systems much smaller distances are used [2.2]. The reference distance should always be in the far-field of the antenna ($d_0 > 2D^2/\lambda$, where D is the largest antenna dimension), so that near-field effects are can be neglected in the reference path loss.

The value of the path loss exponent n depends on the specific propagation environment [2.4]. Table I shows the values of n for different environments [2.3].

Table I. Path-loss exponent values for different environments

Environment	Path Loss Exponent, n
Free space	2
Urban area cellular radio	2.7 to 3.5
Shadowed urban cellular radio	3 to 5
In building, line of sight	1.6 to 1.8
Obstructed in building	4 to 6
Obstructed in factories	2 to 3

Measurements done in environments sharing similar characteristics have shown that the path loss $L_P(d)$ is a random variable that has a lognormal distribution around a mean value $\bar{L}_P(d)$ [2.5]. The mean path loss value, expressed in dB, is:

$$\bar{L}_P(d)|_{dB} = L_{fs}(d_0)|_{dB} + 10n \log\left(\frac{d}{d_0}\right), \quad (9)$$

where the first part is the path loss at the reference distance d_0 , and the second part depends on the distance d and the path-loss exponent n . The path loss $L_P(d)$ (in dB) can also be expressed in terms of the mean $\bar{L}_P(d)$ plus a random variable X_σ , which has a zero mean and a Gaussian distribution [2.6]:

$$L_P(d)|_{dB} = L_{fs}(d_0)|_{dB} + 10n \log\left(\frac{d}{d_0}\right) + X_\sigma|_{dB}. \quad (10)$$

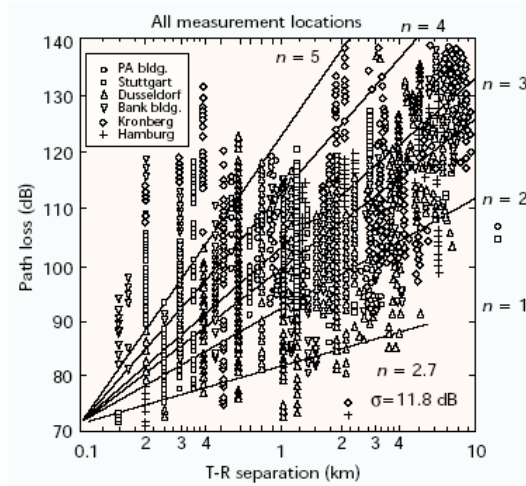


Fig. 5. Path loss vs. distance measured in several German cities⁽²⁾

Formula (10) represents a *lognormal shadowing*; it describes the random shadowing effect that occurs in a large number of measurements of the received power in a large-scale model, at the same distance d between transmitter and receiver, but with different propagation paths [2.5].

Figure 5 shows typical path losses measured in German cities [2.7].

In the following, models for specific aspects of large-scale fade, mentioned in 1.1, are presented.

⁽²⁾ Figure extracted from reference [2.7].

2.1 Reflection

When a radio wave bumps against a smooth surface, whose dimension is large compared with the signal wavelength, the radio wave is partially reflected, partially absorbed, and partially transmitted. While, in fact, the reflected wave is the result of multiple reflections against the wall (Fig. 6), the reflection is usually represented as a single reflection wave; in the following we will adopt this simplification.

When a wave that travels in a first medium impacts with a second medium that is a perfect dielectric, part of the energy is transmitted into the second medium and part comes back to the first medium, without any energy absorption loss. If the second medium is a perfect conductor, then all incident energy is reflected back into the first medium, without any energy loss. The electric field intensity of the reflected and transmitted waves is derived from the incident wave by means of a reflection coefficient (Γ). The reflection coefficient is a function of the material's properties, the wave's polarization, the angle of incidence, and the wave's frequency.

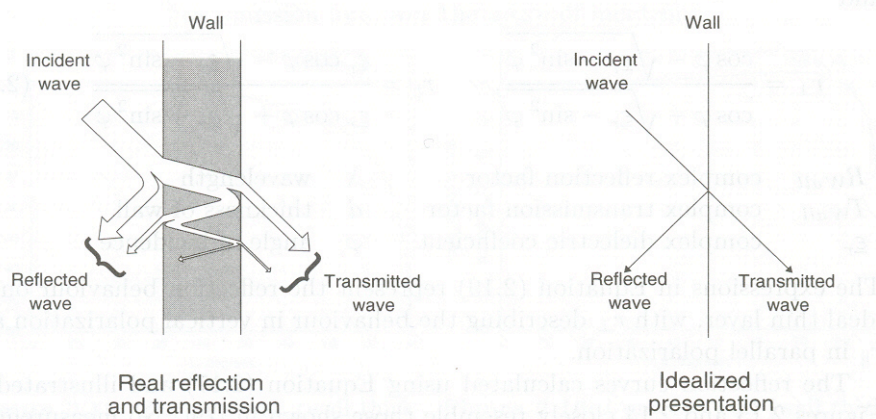


Fig. 6. Reflection at a wall⁽³⁾

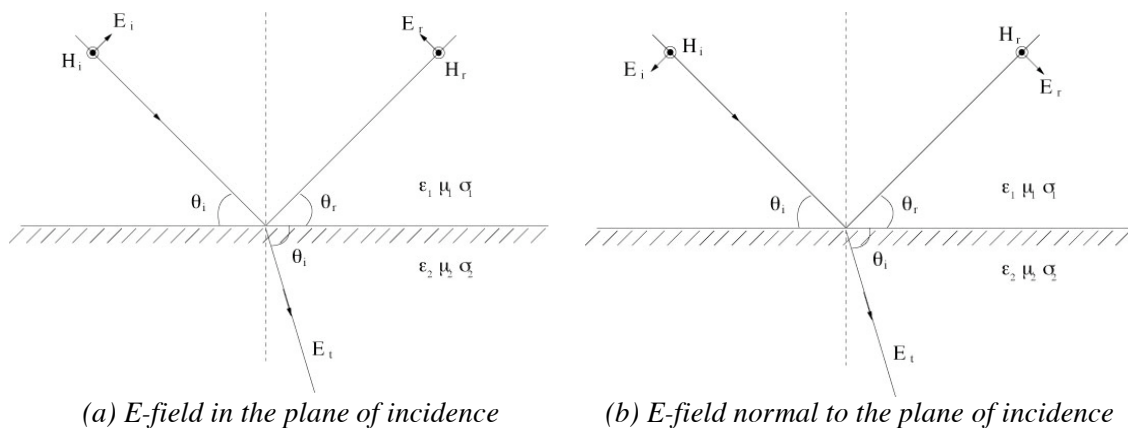


Fig. 7. Geometric scheme for calculating the reflection coefficient between two dielectrics.

In Figure 7, E_i , E_r , E_t are the electric field intensity of the incident wave, the reflected wave, and the transmitted wave, respectively. Parameters ϵ_1 , μ_1 , σ_1 , and ϵ_2 , μ_2 , σ_2 represent the permittivity, permeability, and conductance of the mediums, respectively.

If a material is not perfectly dielectric, the incident energy is partly absorbed: the process can be described by a complex dielectric constant ϵ , defined as

$$\epsilon = \epsilon_0 \epsilon_r - j\epsilon' \quad (11)$$

⁽³⁾ Figure extracted from reference [2.45].

where ϵ_0 is the free space permittivity ($8.85 \cdot 10^{-12}$ Farad/metre), ϵ_r is the relative value of permittivity, $\epsilon' = \sigma / 2\pi f$, where σ is the conductivity of the medium, and f is the frequency of the incident wave.

If the material is a good conductor ($f \ll (\sigma / \epsilon_0 \epsilon_r)$), the terms ϵ_r and σ are insensitive to the frequency. Materials that are not good conductors are called *lossy dielectrics*; for those, ϵ_r is insensitive to the frequency, but this may be not the case for σ , as shown in Table II, derived from [2.8].

Table II. Material parameters at various operating frequency

Material	Relative Permittivity ϵ_r	Conductivity σ (S/m)	Frequency (MHz)
Poor Ground	4	0.001	
Typical Ground	15	0.005	100
Good Ground	25	0.02	100
Sea Water	81	5.0	100
Fresh Water	81	$1 \cdot 10^{-3}$	100
Brick	4.44	$1 \cdot 10^{-3}$	4000
Limestone	7.51	$28 \cdot 10^{-3}$	4000
Glass, Corning 707	4	$18 \cdot 10^{-8}$	1
Glass, Corning 707	4	$27 \cdot 10^{-6}$	100
Glass, Corning 707	4	$5 \cdot 10^{-3}$	10000

The reflection coefficients for the two cases of parallel and perpendicular E-field polarization at the boundary of two dielectrics are given by [2.9]:

$$\Gamma_{\parallel} = \frac{E_r}{E_i} = \frac{\eta_2 \sin \theta_t - \eta_1 \sin \theta_i}{\eta_2 \sin \theta_t + \eta_1 \sin \theta_i} \quad (\text{parallel E - field})$$

$$\Gamma_{\perp} = \frac{E_r}{E_i} = \frac{\eta_2 \sin \theta_i - \eta_1 \sin \theta_t}{\eta_2 \sin \theta_i + \eta_1 \sin \theta_t} \quad (\text{perpendicular E - field}),$$
(12)

where η_i is the intrinsic impedance of the i -th material given by $\sqrt{\mu_i / \epsilon_i}$, and θ_i and θ_t are the angle of the incident wave and of the transmitted wave, respectively. The boundary conditions at the surface of incidence obey Snell's equation:

$$\sqrt{\mu_1 \epsilon_1} \sin(90 - \theta_i) = \sqrt{\mu_2 \epsilon_2} \sin(90 - \theta_t). \quad (13)$$

The boundary conditions, derived from the Maxwell's equations, are used to derive the following equations,

$$\begin{aligned} \theta_i &= \theta_r \\ E_r &= \Gamma E_i \\ E_t &= (1 + \Gamma) E_i, \end{aligned} \quad (14)$$

which mean that the angle of the incident wave is equal to the angle of the reflected wave (θ_r), while the electromagnetic field vector of both the reflected and transmitted waves is proportional to the incident wave. Γ is expressed by Γ_{\parallel} or Γ_{\perp} , depending on whether the E-field is parallel or perpendicular to the boundary of two dielectrics, respectively.

2.1.1 Ground Reflection (2-ray) Model

The *2-ray ground reflection* model assumes that only two paths exist between the transmitter and the receiver: the LOS, and a ground reflected propagation path. The model is based on geometric optics; it is commonly used to predict the large-scale signal strength for mobile radio channels [2.10]. The 2-ray model is valid under the condition that $d \gg \sqrt{h_t h_r}$ [2.9]; the meaning of h_t and h_r it explained in Fig. 8, which describes the model.

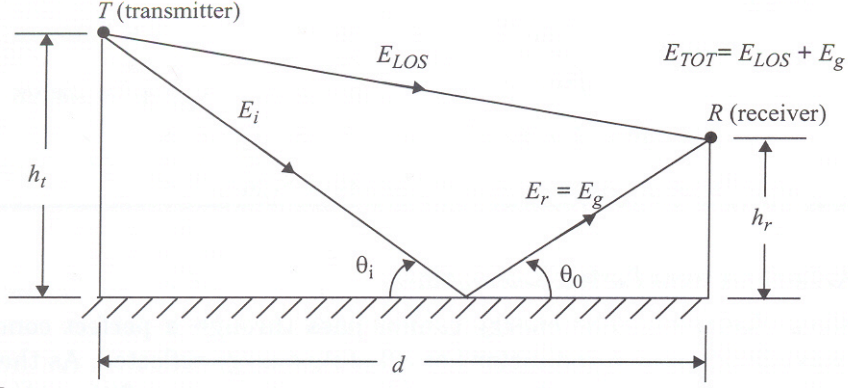


Fig. 8. 2-ray ground reflection model⁽⁴⁾.

In Fig. 8, E_g is the electric field intensity of the reflected wave, E_{LOS} is the electric field intensity of the straight wave, and θ_0 is the angle between the ground and the reflected wave.

With the help of Fig. 8, the path length difference of the two components can be computed as

$$\Delta d = \sqrt{d^2 + (h_t + h_r)^2} - \sqrt{d^2 + (h_t - h_r)^2}. \quad (15)$$

The phase difference θ_Δ between the two E-field components and the time delay τ_Δ between the components are computed as

$$\theta_\Delta = \frac{2\pi\Delta d}{\lambda} \quad \text{and} \quad \tau_\Delta = \frac{\Delta d}{c}, \quad (16)$$

respectively, where c is the speed of light. The received E-field is obtained by:

$$E = E_0 \left[1 + |\Gamma| e^{j(\bar{\Gamma} - \theta_\Delta)} \right] = E_0 \left\{ 1 + |\Gamma| \cos(\bar{\Gamma} - \theta_\Delta) + j|\Gamma| \sin(\bar{\Gamma} - \theta_\Delta) \right\}, \quad (17)$$

where E_0 is the E-field of the LOS component at the receiver, and Γ is the reflection coefficient. The power at the receiver is given by

$$P \propto |E_0|^2 \left\{ 1 + |\Gamma|^2 + 2|\Gamma|^2 \cos(\bar{\Gamma} - \theta_\Delta) \right\} \quad (18)$$

By using this model, it derives that the received power is inversely proportional to d^4 , when $d \gg \sqrt{h_t h_r}$ [2.3, 2.46].

2.2 Diffraction

Diffraction describes the modifications of propagating waves when obstructed. This phenomenon allows radio waves to propagate around the bending of the earth and behind obstructions. Let an obstruction be at a distance d_1 from the transmitter (T) and d_2 from the receiver (R), as shown in Fig. 9; the signal arrives at the receiver even if the LOS path does not exist.

In order to study the diffraction phenomenon, it is important to define a *wave front*, which is the surface defined by the locus of points that have the same phase and the same path length from the source. The wave front is perpendicular to the ray that represents an electromagnetic wave.

⁽⁴⁾ Figure extracted from reference [2.9].

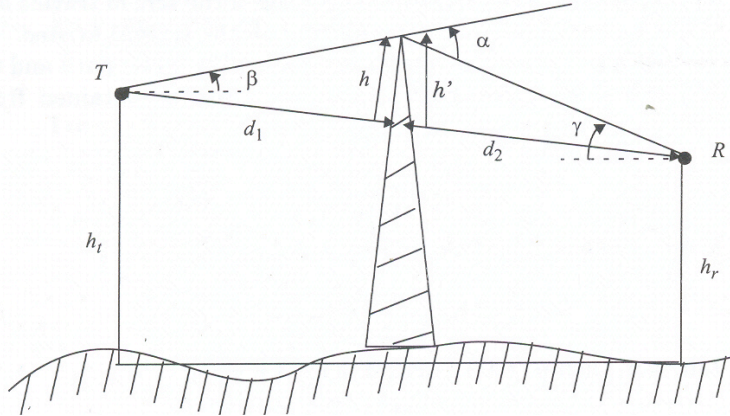


Fig. 9. Knife-edge diffraction geometry when the transmitter and receiver are not at the same height. Note that if the angles α and β are small and $h \ll d_1$ and $h \ll d_2$, then h and h' are virtually identical⁽⁴⁾.

We face the problem by using Huygens' principle [2.11]. If we consider an infinitesimal surface A in the wave front, the E-field generated at the receiver R by A depends on the distance between A and R and on the angle θ (Fig. 10). The phase of the E-field also depends on the distance between A and R .

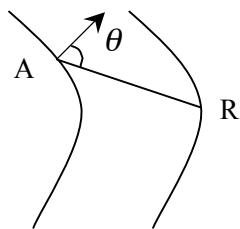


Fig. 10. E-field generated in R by A .

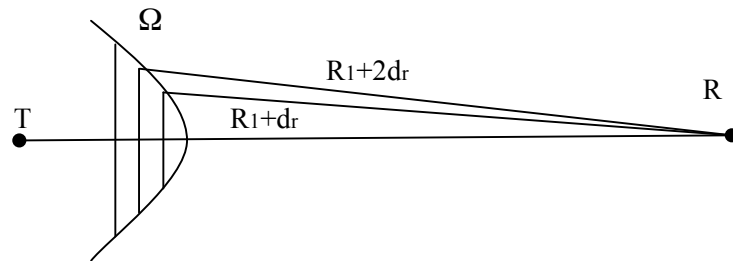


Fig. 11. E-field generated in R by all infinitesimal elements.

In order to calculate the E-field in R , we must consider every infinitesimal element A on the surface Ω , and add up all the E-fields (Fig. 11) generated by each element.

Figure 12 shows the vector sum of the E-fields, where d_r is the infinitesimal increment of distance. The vector sum increases in module as far as $d_r = \lambda/2$, where its phase is π , and then decreases as far as $d_r = \lambda$, where its phase is 2π .

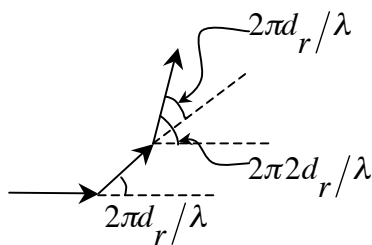


Fig. 12. Vector sum of the E-field.

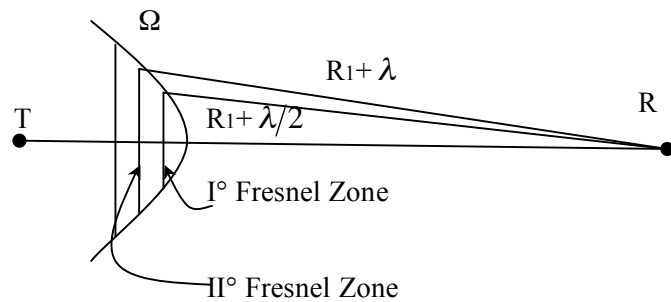


Fig. 13. Fresnel zone

The *Fresnel zones* represent successive regions where the path length difference of the secondary waves with respect to the LOS path is a multiple of $\lambda/2$ (Fig. 13). The Fresnel zones explain the concept of diffraction-loss as a function of the path difference around an obstruction. If a signal bumps against a perfectly absorbent surface, as shown in Fig. 14, the E-field at the receiver changes as a function of ρ , as shown in Fig. 15.

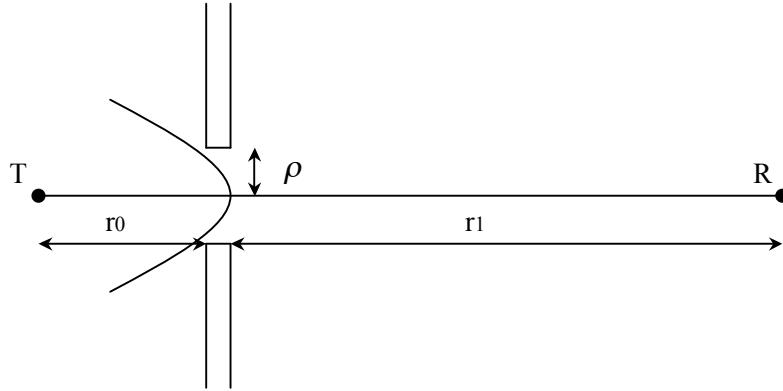


Fig. 14. Perfect absorbent surface with an opening between transmitter and receiver

In Fig. 15, E_0 is the E-field at the receiver in the absence of both the obstacle and the ground. We can see that the E-field increases up to the first Fresnel zone; then it decreases up to the second Fresnel zone, and so on. The values of ρ for the K^{th} -Fresnel zone are

$$\rho_K = \sqrt{\lambda K \frac{r_0 r_1}{d}} \quad (19)$$

where K is the order of the Fresnel zone and d is the distance between transmitter and receiver.

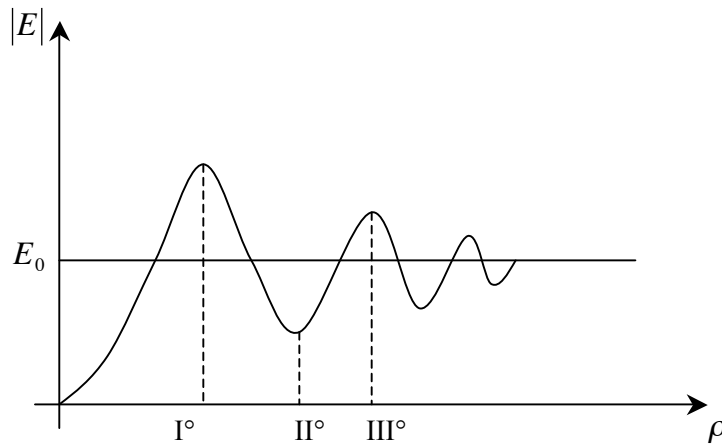


Fig. 15. E-field versus height of the opening

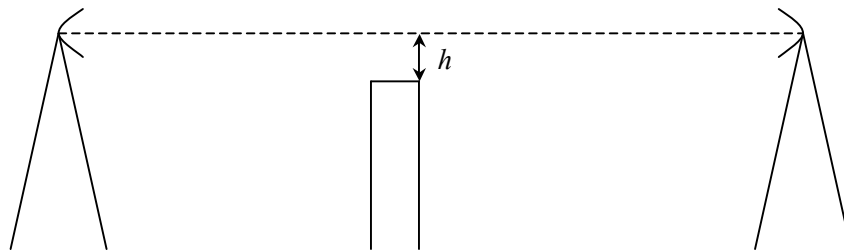


Fig. 16. Obstacle between transmitter and receiver

When the obstacle is as shown in Fig. 16, the E-field appears as in Fig. 17. We can see that the amplitude of the oscillation is smaller than in the case shown in Fig. 14.

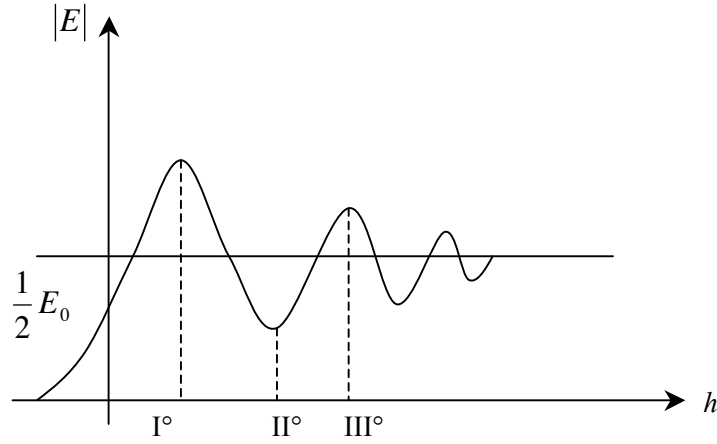


Fig. 17. E-field versus height between line of sight and obstacle (h)

2.2.1 Knife-edge Diffraction model

Estimating the signal attenuation caused by diffraction of radio waves over buildings is essential in predicting the field strength that arrives at the receiver. When a single object, as a hill or a building, causes shadowing, the attenuation due to diffraction can be seen as the attenuation caused by the Knife-edge [2.9]. In other words, the obstruction can be treated as a knife-edge. Let us consider a transmitter and a receiver separated in free space as shown in Fig. 18a. Let an obstructing screen of effective height with infinite width be placed between them at distance d_1 from the transmitter, and d_2 from the receiver. It is important to introduce the dimension-less *Fresnel-Kirchoff diffraction parameter* ν [2.12]:

$$\nu = h \sqrt{\frac{2(d_1 + d_2)}{\lambda d_1 d_2}} \quad (20)$$

If we consider a receiver R located in the shadowed region (also called *diffraction zone*), the field strength at point R , in Fig. 18, is a vector sum of the fields due to all the secondary Huygens' sources in the plane above the knife-edge. The E-field strength E_d of the knife-edge diffraction is given by

$$\frac{E_d}{E_0} = F(\nu) = \frac{(1+j)}{2} \int_{\nu}^{\infty} \exp\left(-\frac{j\pi t^2}{2}\right) dt \quad (21)$$

where E_0 is the free-space field strength in the absence of both the obstacle and the ground, and $F(\nu)$ is a function of the Fresnel-Kirchoff diffraction parameter.

$F(\nu)$ is commonly evaluated by using tables or graphs. The diffraction gain due to the presence of a knife-edge is commonly used; it is given by:

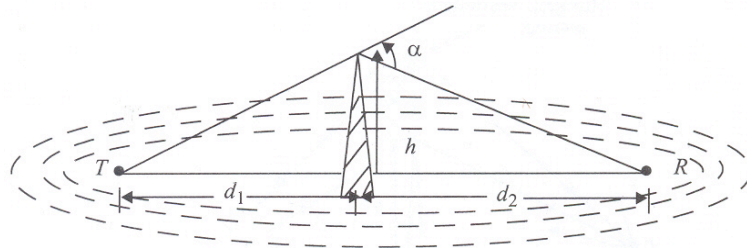
$$G_d|_{dB} = 20 \log|F(\nu)| \quad (22)$$

A graphical representation of $G_d(dB)$ as a function of ν is given in Fig. 19. An approximate solution for the above equation is provided by [2.13]:

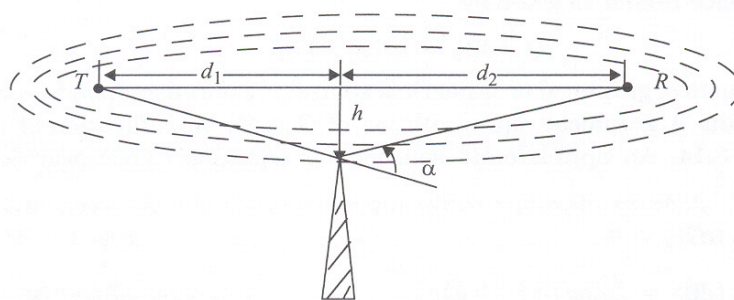
$$\begin{aligned} G_d|_{dB} &= 0 & \nu &\leq -1 \\ G_d|_{dB} &= 20 \log(0.5 - 0.62\nu) & -1 &\leq \nu \leq 0 \\ G_d|_{dB} &= 20 \log(0.5 \exp(-0.95\nu)) & 0 &\leq \nu \leq 1 \\ G_d|_{dB} &= 20 \log\left(0.4 - \sqrt{0.1184 - (0.38 - 0.1\nu)^2}\right) & 1 &\leq \nu \leq 2.4 \end{aligned} \quad (23)$$

$$G_d|_{dB} = 20 \log\left(\frac{0.225}{v}\right) \quad v > 2.4$$

The approximation of a path profile by *multiple knife edges (MKE)* is a frequently applied refinement. Techniques to estimate the loss over such a sequence of knife edges have been proposed by Bullington [2.14], Deygout [2.15], Epstein, and Peterson [2.16].



(a) α and v are positive, as h is positive



(b) α and v are negative, as h is negative

Fig. 18. Knife-edge diffraction model⁽⁴⁾

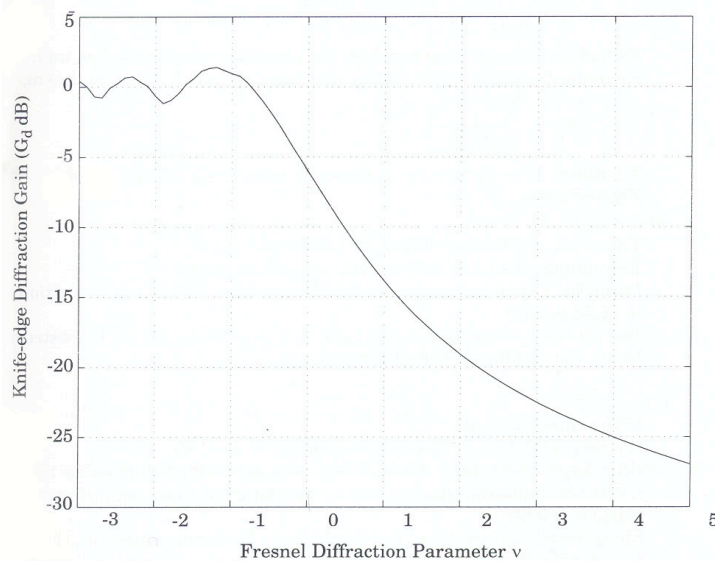


Fig. 19. A graphical representation of $G_d(dB)$ as a function of v ⁽⁴⁾.

2.3 Scattering

In mobile radio environment the signal level is often unlike what is predicted by reflection and diffraction models. This happens because the signal bumps against a rough surface, and the reflected energy spreads in all directions due to scattering. Objects, such as lamppost or trees, tend to scatter energy in all directions.

2.3.1 Radar Cross Section Model

In a radio channel, the knowledge of the location of the object that causes scattering can be used to predict the scattered signal strengths. The *radar cross section (RCS)* is defined as the ratio between the power density of the signal, scattered in the direction of the receiver, and the power density of the radio wave incident upon the scattering object, expressed in square meters*.

For rural and macro cellular areas, some of the models that have shown the best performance are models that use *bistatic radar techniques* [2.17, 2.18]. Models based on the *bistatic radar equation* may be used to calculate the received power due to scattering. The bistatic radar equation describes the scattering phenomenon as

$$P_R|_{dBm} = P_T|_{dBm} + G_T|_{dBi} + 20\log(\lambda) + RCS|_{dB\cdot m^2} - 30\log(4\pi) - 20\log d_T - 20\log d_R \quad (24)$$

where dBi is the dB ratio between the actual power with respect to an isotropic radiator, d_T and d_R are the distances of the scattering object from the transmitter and the receiver, respectively. In (24), the scattering object is assumed in a far field region, also called Fraunhofer region, (if $r > 2D^2/\lambda$, where D is the dimension of the antenna) of both transmitter and receiver. This model is useful for predicting the received power that scattered off large objects, such as buildings [2.19 – 2.21].

2.4 Outdoor propagation models

When the radio communications take place over irregular terrain, the terrain profile, with the presence of trees, buildings and other obstacles, changes the estimation of the path loss. Many models exist that are adequate to predict the path loss, and the following methods widely vary in their approach and accuracy.

2.4.1 Longley-Rice model

The Longley-Rice model [2.22, 2.23] is applicable to point-to-point communication systems in the frequency range from 40 MHz to 100 GHz, over different kinds of terrain. The average transmission loss is predicted by using the path geometry of the terrain profile and the refractivity of the troposphere. Geometric optics techniques (primarily the 2-Ray ground reflection model) are used to predict signal strengths within the radio horizon. Diffraction losses over isolated obstacles are estimated by using the Fresnel-Kirchoff knife-edge models. The Longley-Rice model is also available as a computer program [2.24] to calculate large-scale average transmission loss relative to free space loss over irregular terrain for frequencies between 20 MHz and 10GHz. For a given transmission path, the program takes as inputs the transmission frequency, path length, polarization, antenna heights, surface reflectivity and climate. The program also operates on path specific parameters such as the horizon distance of the antennas, the horizon elevation angle, and other specific inputs.

The Longley-Rice model operates in two modes. When a detailed terrain path profile is available, the path specific parameters can be easily determined and the prediction is called *point-to-point mode* prediction. On the other hand, if the terrain path profile is not available, the Longley-Rice method provides techniques to estimate the path specific parameters, and such a prediction is called an *area mode* prediction.

There have been many modifications and corrections to the Longley-Rice model since its original publications. One important modification [2.24] deals with radio propagation in urban areas, and this is particularly relevant to mobile radio. This modification introduces an excess term as an allowance for the additional attenuation due to urban clutter near the receiving antenna. This extra term, called the *urban factor (UF)*, has been derived by comparing the predictions in the original Longley-Rice model with those obtained by Okumura [2.25].

* RCS can be viewed as a comparison between the reflected signal strength from a target and the reflected signal from a perfectly smooth sphere of cross sectional area of 1 m^2 .

One shortcoming of the Longley-Rice model is that it does not provide a way of determining corrections due to environmental factors in the immediate vicinity of the mobile receiver, or to consider correction factors in order to account for the effects of buildings and foliage.

2.4.2 Okumura model

Okumura's model is one of the most widely used models for signal prediction in urban areas. In 1965 Okumura carried out extensive measurements around Tokyo in the frequency range from 150 MHz to 2 GHz. Okumura published the results of his measurements as curves [2.26], given the median attenuation relative to the free space L_F , in an urban area, with a base station antenna height h_t of 200 meters and a mobile antenna height h_r of 3 meters. These curves were plotted as a function of the frequency and the distance from the base station. To find the path loss by using the Okumura's model, the free space path loss between transmitter and receiver is computed; then, the value of $A_{mu}(f, d)$, which is the median attenuation relative to free space, is added with the correction factor of the antenna height gain. The model is described by:

$$L = L_F + A_{mu}(f, d) + G(h_t) + G(h_r) - G_{AREA} \quad (25)$$

where L is the average propagation loss in dB, L_F the free-space propagation loss, $G(h_t)$ is the base station antenna height gain factor, $G(h_r)$ is the mobile antenna height gain factor, and G_{AREA} is the gain due to the type of environment. Plots of $A_{mu}(f, d)$ and G_{AREA} for a wide range of frequencies are shown in Figs 20 and 21, respectively.

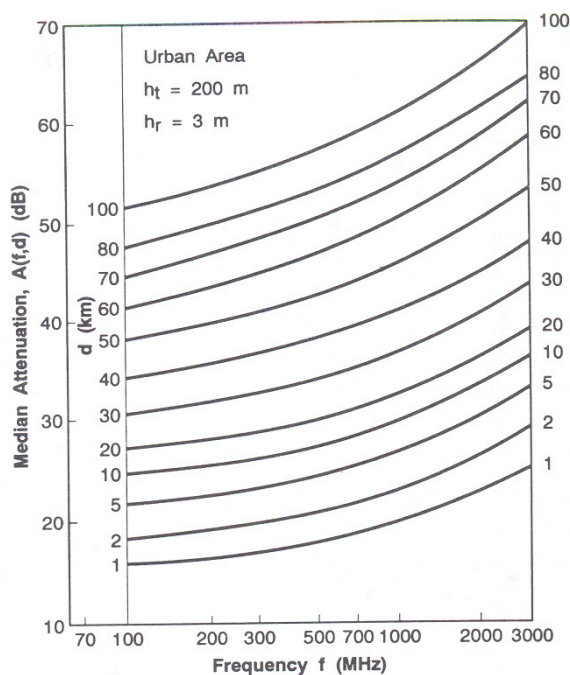


Fig. 20. Median attenuation relative to free space, over a quasi-smooth terrain⁽⁵⁾.

Other corrections may also be applied to Okumura's model. Some of the important terrain-related parameters are the terrain undulation height, the isolated ridge height, the average slope of terrain, and mixed land-sea parameter. Once the terrain-related parameters are calculated, the necessary correction factors can be added or subtracted, as required. All these correction factors are also available as Okumura curves [2.25]. Okumura's model is entirely based on measured data, and does not provide any analytical explanation.

⁽⁵⁾ Figure extracted from reference [2.26].

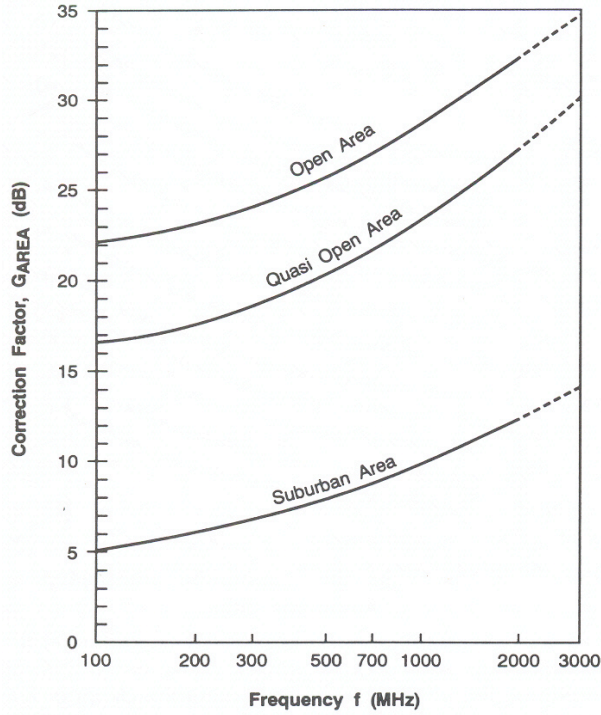


Fig. 21. Correction factor for different types of terrain⁽⁵⁾.

2.4.3 Hata model

The Hata model (1980) is an empirical formulation of the curves provided by Okumura, approximated through analytical formulations [2.27]. Hata presents the urban area path loss and supplies a correction factor to the formula for applying it to other situations. The formula for the median path loss in urban areas is given by

$$L(\text{urban}) = 69.55 + 26.16 \log f_c - 13.82 \log h_t - a(h_r) + (44.9 - 6.55 \log h_t) \log d \quad (26)$$

where the path loss is expressed in dB, f_c is the frequency in the range 150-1500 MHz, h_t is the effective transmitter antenna height ranging from 30 to 200 meters, h_r is the effective receiver antenna height ranging from 1 to 10 meters, d is the distance between transmitter and receiver in km, and $a(h_r)$ is the correction factor for the effective receiver antenna height, which depends on the environment. For a small or medium city, the correction factor is given by

$$a(h_r) = (1.1 \log f_c - 0.7) h_r - (1.56 \log f_c - 0.8) \quad (27)$$

while, for a large city, it is given by

$$\begin{aligned} a(h_r) &= 8.29(\log 1.54 h_r)^2 - 1.1 && \text{for } f_c \leq 200 \text{ MHz} \\ &= 3.2(\log 11.75 h_r)^2 - 4.97 && \text{for } f_c \geq 400 \text{ MHz} \end{aligned} \quad (28)$$

2.4.4 Extension to Hata model

The European CO-operation for Scientific and Technical research (EURO-COST) formed the COST-231 working committee to develop an extended version of the Hata model. COST-231 proposed the following formula to extend Hata's model to 2 GHz. The proposed model for path loss [2.28] is:

$$L(\text{urban}) = 46.3 + 33.9 \log h_t - a(h_r) + (44.9 - 6.55 \log h_t) \log d + C_M \quad (29)$$

where $a(h_r)$ is defined in equations (27) and (28), and

$$C_M = \begin{cases} 0 \text{ dB} \\ 3 \text{ dB} \end{cases} \quad (30)$$

where the value of 0 is for medium-sized city and suburban areas, and 3 for metropolitan centers. The COST-231 extension of the Hata model is restricted to the following ranges of parameters:

- f : 1500MHz to 2000MHz
- h_t : 30 m to 200 m
- h_r : 1m to 10 m
- d : 1Km to 20 Km

2.4.5 Walfisch and Bertoni model

A model developed by Walfisch and Bertoni [2.29] considers the impact of rooftops and building heights by using diffraction in order to predict average signal strengths at street level. The model considers the path loss, S , to be a product of three factors:

$$S = L_0 L_{rts} L_{ms} \quad (31)$$

where L_0 represents the free space path loss between isotropic antennas, at a distance R :

$$L_0 = \left(\frac{4\pi R}{\lambda} \right)^2 \quad (32)$$

The path loss, expressed in dB, is given by

$$S|_{dB} = L_0 + L_{rts} + L_{ms} \quad (33)$$

where L_{rts} the *rooftop to street diffraction and scatter loss*, and L_{ms} indicates the multi-screen diffraction loss due to rows of buildings [2.30].

Figure 22 illustrates the geometry used in the Walfisch Bertoni model [2.29], [2.31]. This model was considered for ITU-R (International Telecommunication Union - Radio communications) use in the IMT-2000 (International Mobile Telecommunications-2000) standards activities [2.32, 2.33].

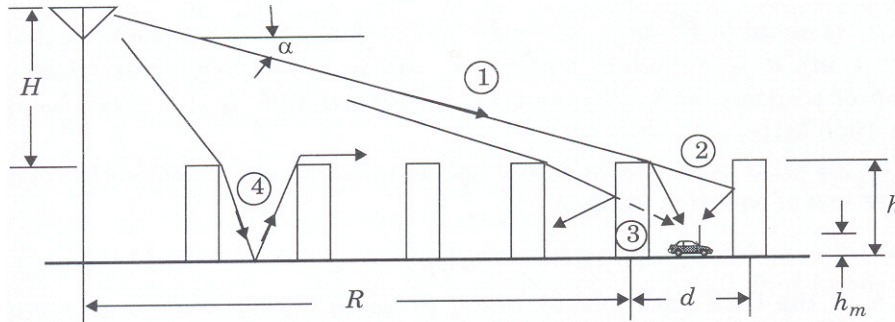


Fig. 22. Propagation geometry for the model proposed by Walfisch and Bertoni⁽⁶⁾.

2.4.6 Wideband Model

Feuerstein used a 20 MHz-pulsed transmitter at 1900 MHz to measure the path loss, outage, and delay spread in typical microcellular systems. Using base station antenna heights (h_t) of 3.7 m, 8.5 m, and 13.3 m, and a mobile receiver with an antenna height (h_r) of 1.7 m above ground, statistics for path loss, multipath, and coverage area were inferred from extensive measurements in LOS and obstructed (OBS) environments [2.10]. This work revealed that a 2-Ray ground reflection model is a good estimate for path loss in LOS, and a simple log-distance path loss model holds well for OBS environments (9).

For a flat ground reflection model, the distance d_f at which the first Fresnel zone just becomes obstructed by the ground (*first Fresnel zone clearance*) is given by

$$d_f = \frac{1}{\lambda} \sqrt{16h_t^2 h_r^2 - \lambda^2 (h_t^2 + h_r^2)} + \frac{\lambda^4}{16} \quad (34)$$

⁽⁶⁾ Figure extracted from reference [2.29].

For LOS cases, a double regression path loss model that uses a regression breakpoint at the first Fresnel zone was shown to fit well to measurements. The model assumes omni-directional vertical antennas and predicts the average path loss as

$$\bar{L}_p(d) = \begin{cases} 10n_1 \log(d) + p_1 & \text{for } 1 < d < d_f \\ 10n_2 \log(d/d_f) + 10n_1 \log(d_f) + p_1 & \text{for } d > d_f \end{cases} \quad (35)$$

where p_1 is equal to the path loss in dB at the reference distance of $d_0 = 1$ meter, d is the distance in meters between receiver and transmitter, n_1 and n_2 are path loss exponents, which are a function of the transmitter height, as given in Table III.

For the OBS case, the path loss was found to fit the standard log-distance path loss law:

$$\bar{L}_p(d) = 10n \log(d) + p_1 \quad (36)$$

where n is the OBS path loss exponent given in Table III as a function of the transmitter height. Table III indicates that the lognormal shadowing component is between 7.5 and 9.5 dB, regardless of the antenna height, and that LOS environments provide slightly less path loss than the 2-Ray model, for which $n_1 = 2$ and $n_2 = 4$.

Table III. Parameters for the wideband microcell model, at 1900 MHz (from [2.10]).

Transmitter antenna height	1900 MHz LOS			1900 MHz OBS	
	n_1	n_2	σ [dB]	n	σ [dB]
Low (3.7 m)	2.18	3.29	8.76	2.58	9.31
Medium (8.5 m)	2.17	3.36	7.88	2.56	7.67
High (13.3 m)	2.07	4.16	8.77	2.69	7.94

Table IV summarizes the characteristics of the considered outdoor propagation models.

Table IV. Characteristics of the considered outdoor propagation models.

Models	Frequency range	Characteristics
Longley-Rice	40MHz-100GHz	<ul style="list-style-type: none"> Path loss is predicted by using the path geometry of the terrain profile. Geometric optics techniques are used to predict signal strengths within the radio horizon. Diffraction losses over isolated obstacles are estimated by using the Fresnel-Kirchoff knife-edge model.
Okumura	150MHz-2GHz	<ul style="list-style-type: none"> One of the most widely used models for signal prediction in urban areas. Okumura published the results of his extensive measurement campaign as curves, given the median attenuation relative to the free space with a base station antenna height of 200 meters and a mobile antenna height of 3 meters.
Hata	150MHz-1.5GHz	<ul style="list-style-type: none"> Empirical formulation of the curves provided by Okumura, approximated through analytical formulations. Hata presents the urban area path loss and supplies a correction factor for applying his formula to other situations.
Extention to Hata	1.5GHz-2GHz	<ul style="list-style-type: none"> COST-231 proposed a formula to extend Hata's model to 2 GHz.
Walfisch-Bertoni		<ul style="list-style-type: none"> This model considers the impact of rooftops and building heights by using diffraction in order to predict average signal strengths at street level.
Wideband		<ul style="list-style-type: none"> 2-Ray ground reflection model is a good estimate for path loss in LOS log-distance path loss model performs well for OBS environments.

2.5 Indoor propagation models

There is a great interest in characterizing the radio communications channel inside a building. The indoor channel differs from the outdoor channel because of the variation in the fading rate and the type of interference. The delay spread (see Appendix) in the indoor radio channel is typically smaller than the one in the outdoor channel; moreover, movements inside a building are often smaller than movements of vehicles in an urban area. Therefore, the change in channel characteristics is slower in time. The interference types are different because the propagation within the buildings is strongly influenced by local features, such as construction materials and type of building. The field of indoor radio propagation is relatively new, with the first wave of research occurring in the early 1980. Cox [2.34] at AT&T Bell Laboratories and Alexander [2.35] at British Telecom were the first to carefully study indoor path loss in and around a large number of houses and office buildings. Literature surveys are available on the topic of indoor propagation [2.36, 2.37].

Buildings have a wide variety of partitions and obstacles that form the internal and external structure. Houses and office buildings typically use a different partition and often have different size. Partitions that are formed as a part of the building structure are called *hard partitions*, while partitions that may be moved are called *soft partitions*. Partitions widely vary in their physical and electrical characteristics, thus making it difficult to apply general models to specific indoor installations. Nevertheless, researchers have created extensive databases of losses for a great number of partitions, as shown in Table V.

Table V. Average signal loss measurements reported by various researchers for radio paths obstructed by common building material.

Material Type	Loss (dB)	Frequency	Reference
All metal	26	815MHz	[2.34]
Aluminium siding	20.4	815MHz	[2.34]
Foil insulation	3.9	815MHz	[2.34]
Concrete block wall	13	1300MHz	[2.43]
Loss from one floor	20-30	1300MHz	[2.43]
Loss from one floor and one wall	40-50	1300MHz	[2.43]
Fade observed when transmitter turned a right angle corner in a corridor	10-15	1300MHz	[2.43]
Light textile inventory	3-5	1300MHz	[2.43]
Chain-like fenced in area 20 ft high containing tools, inventory, and people	5-12	1300MHz	[2.43]
Metal blanket – 12 sq ft	4-7	1300MHz	[2.43]
Metallic hoppers which hold scrap metal for recycling – 10 sq ft	3-6	1300MHz	[2.43]
Small metal pole – 6" diameter	3	1300MHz	[2.43]
Metal pulley system used to hoist metal inventory – 4 sq ft	6	1300MHz	[2.43]
Light machinery < 10 sq ft	1-4	1300MHz	[2.43]
General machinery – 10 – 20 sq ft	5-10	1300MHz	[2.43]
Heavy machinery > 20 sq ft	10-12	1300MHz	[2.43]
Metal catwalk/stairs	5	1300MHz	[2.43]
Light textile	3-5	1300MHz	[2.43]
Heavy textile inventory	8-11	1300MHz	[2.43]
Area where workers inspect metal finished products for defects	3-12	1300MHz	[2.43]
Metallic inventory	4-7	1300MHz	[2.43]
Concrete block wall	13-20	1300MHz	[2.43]
Ceiling duct	1-8	1300MHz	[2.43]
Concrete wall	8-15	1300MHz	[2.43]
Concrete floor	10	1300MHz	[2.43]

Commercial absorber	38	9.6 GHz	[2.44]
Commercial absorber	51	28.8 GHz	[2.44]
Commercial absorber	59	57.6 GHz	[2.44]
Dry plywood – 1 sheet	1	9.6 GHz	[2.44]
Dry plywood – 1 sheet	4	28.8 GHz	[2.44]
Dry plywood – 1 sheet	8	57.6 GHz	[2.44]
Dry plywood – 2 sheet	4	9.6 GHz	[2.44]
Dry plywood – 2 sheet	6	28.8 GHz	[2.44]
Dry plywood – 2 sheet	14	57.6 GHz	[2.44]
Wet plywood – 1 sheet	19	9.6 GHz	[2.44]
Wet plywood – 1 sheet	32	28.8 GHz	[2.44]
Wet plywood – 1 sheet	59	57.6 GHz	[2.44]
Wet plywood – 2 sheet	39	9.6 GHz	[2.44]
Wet plywood – 2 sheet	46	28.8 GHz	[2.44]
Wet plywood – 2 sheet	57	57.6 GHz	[2.44]

The losses at the floors of a building depend on the material of the buildings, as well as the type of construction used to create the floors [2.38] [2.39]. Table VI illustrates values for the *floor attenuation factor* (FAF) in three buildings in San Francisco [2.38]. It can be seen that for all three buildings the attenuation at one floor is greater than the incremental attenuation caused by each additional floor. Table VII illustrates very similar tendencies; after four or five separations, very little additional path loss is experienced.

Table VI. Total Floor Attenuation Factor and standard deviation σ (dB) for three buildings. Each point represents the average path loss over a 20λ measurement track [2.38]

Building	915 MHz FAF (dB)	σ (dB)	Number of locations	1900 MHz FAF (dB)	σ (dB)	Number of locations
Walnut Creek						
One floor	33.6	3.2	25	31.3	4.6	110
Two Floors	44	4.8	39	38.5	4	29
SF PacBell						
One floor	13.2	9.2	16	26.2	10.5	21
Two Floors	18.1	8	10	33.4	9.9	21
Three Floors	24.0	5.6	10	35.2	5.9	20
Four Floors	27.0	6.8	10	38.4	3.4	20
Five Floors	27.1	6.3	10	46.4	3.9	17
San Ramon						
One floor	29.1	5.8	93	35.4	6.4	74
Two Floors	36.6	6	81	35.6	5.9	41
Three Floors	39.6	6	70	35.2	3.9	27

Table VII. Average Floor Attenuation Factor in dB for one, two, three, and four floors in two office buildings [2.39]

Building	FAF (dB)	σ (dB)	Number of locations
Office Building 1:			
Through One Floor	12.9	7	52
Through Two Floors	18.7	2.8	9
Through Three Floors	24.4	1.7	9
Through Four Floors	27	1.5	9
Office Building 2:			
Through One Floor	16.2	2.9	21
Through Two Floors	27.5	5.4	21
Through Three Floors	31.6	7.2	21

In general, indoor channels may be classified either as LOS or obstructed, with varying degrees of clutter [2.40]. In the following, we will present some of the recently emerged models recently emerged.

2.5.1 Log-distance path loss model

Many researchers have shown that indoor path loss obeys the distance power law:

$$L_P(d)|_{dB} = L_{fs}(d_0)|_{dB} + 10n \log\left(\frac{d}{d_0}\right) + X_\sigma|_{dB} \quad (37)$$

where $L_P(d_0)$ is the path loss, $L_{fs}(d_0)$ is the path loss in free space at distance d_0 , n depends on the surroundings and building type, and X_σ represents a normal random variable (in dB) with a standard deviation of σ dB. Notice that (37) is identical in form to the lognormal shadowing model of (10). Typical values of n for various building are provided in Table VIII [2.41].

Table VIII. Path loss exponent and standard deviation measured in different buildings [2.31].

Building	Frequency (MHz)	n	σ (dB)
Retail Stores	914	2.2	8.7
Grocery Store	914	1.8	5.2
Office, hard partition	1500	3	7
Office, soft partition	900	2.4	9.6
Office, soft partition	1900	2.6	14.1
Factory LOS			
Textile/Chemical	1300	2	3
Textile/Chemical	4000	2.1	7
Paper/Cereals	1300	1.8	6
Metalworking	1300	1.6	5.8
Suburban Home			
Indoor Street	900	3	7
Factory OBS			
Textile/Chemical	4000	2.1	9.7
Metalworking	1300	3.3	6.8

2.5.2 Attenuation factor model

An in-building propagation model that includes the effect of building type, as well as the variations caused by obstacle, was described by Seidel in [2.39]. The attenuation factor model is given by

$$L_P(d)|_{dB} = L_{fs}(d_0)|_{dB} + 10n_{SF} \log\left(\frac{d}{d_0}\right) + FAF|_{dB} \quad (38)$$

where n_{SF} represents the exponent value for the “same floor” measurement. Thus, if a good estimate for n exists (e.g., selected from table VIII) for the same floor, the path loss on the different floor can be predicted by adding an appropriate value of FAF. Alternatively, in equation (38) FAF may be replaced by an exponent that considers the effects of multiple floor separation:

$$L_P(d)|_{dB} = L_{fs}(d_0)|_{dB} + 10n_{MF} \log\left(\frac{d}{d_0}\right) \quad (39)$$

where n_{MF} denotes a path loss exponent based on measurements through multiple floors. Table IX illustrates typical values of n for a wide range of locations in many buildings. This table also illustrates how the standard deviation decreases as the average region becomes smaller.

Figure 23 shows the measured path loss in two multi-floor office buildings.

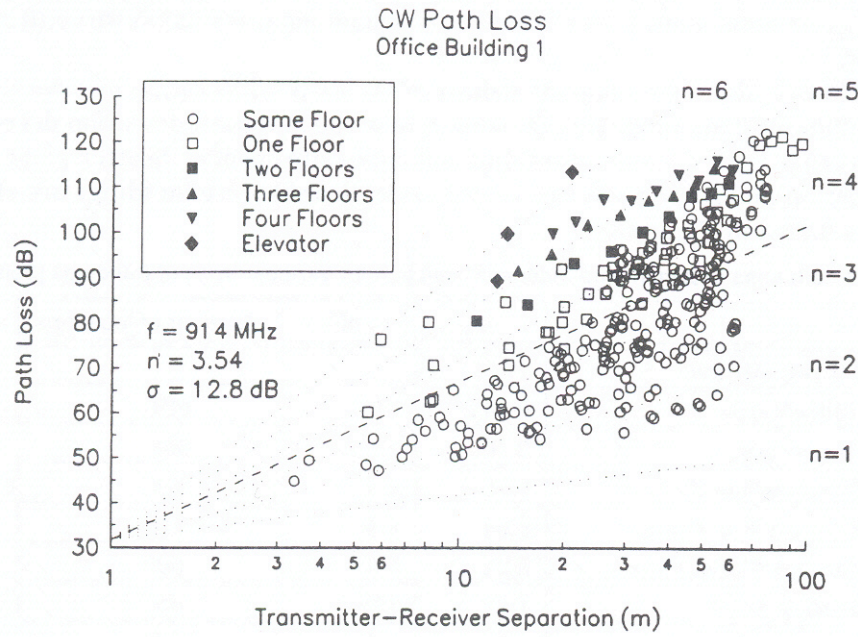


Fig. 23. Scatter plot of path loss as a function of distance in Office Building 1⁽⁷⁾.

Table IX. Path loss exponents and standard deviation for various types of buildings [2.39]

	n	σ (dB)	Number of locations
All Buildings:			
All locations	3.14	16.3	634
Same Floor	2.76	12.9	501
Through One Floor	4.19	5.1	73
Through Two Floors	5.04	6.5	30
Through Three Floors	5.22	6.7	30
Grocery Store	1.81	5.2	89
Retail Store	2.18	8.7	137
Office Building 1:			
Entire Building	3.54	12.8	320
Same Floor	3.27	11.2	238
West Wing 5 th Floor	2.68	8.1	104
Central Wing 5 th Floor	4.01	4.3	118
West Wing 4 th Floor	3.18	4.4	120
Office Building 2:			
Entire Building	4.33	13.3	100
Same Floor	3.25	5.2	37

Devasirvatham et. al., in [2.42], found that in-building path loss obeys free space plus an additional loss factor which increases exponentially with the distance, as shown in Table X. Based on this work in multi-floor buildings it would be possible to modify the equation (38) as follows:

$$L_P(d)|_{dB} = L_{fs}(d_0)|_{dB} + 20 \log\left(\frac{d}{d_0}\right) + \alpha d + FAF|_{dB} \quad (40)$$

where α is the attenuation constant for the channel in units of dB per meter (dB/m). Table X provides typical value of α as a function of frequency as measured in [2.41].

⁽⁷⁾ Figure extracted from reference [2.38].

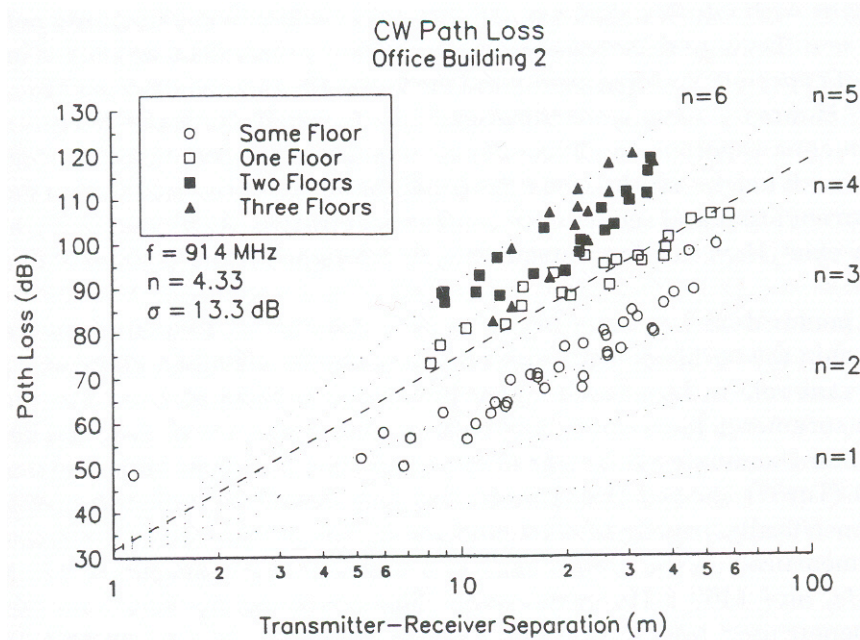


Fig. 24. Scatter plot of path loss as a function of distance in Office Building 2⁽⁷⁾.

Table X. Free space plus linear path attenuation model [2.42]

Location	Frequency	Attenuation (dB/m)
Building 1: 4 storey	850 MHz	0.62
	1.7 MHz	0.57
	4 GHz	0.47
Building 1: 4 storey	850 MHz	0.48
	1.7 MHz	0.35
	4 GHz	0.23

III. The terrestrial wireless Small-scale propagation models

The *small scale fading* models are used to describe short-term, rapid amplitude fluctuations of the received signal during a short period of time. This fading is caused by interference between two or more multipath components that arrive at the receiver while the mobile travels a short distance (a few wavelengths) or over a short period of time. These waves combine vectorially at the receiver, and the resulting signal can rapidly vary in amplitude and phase [3.1].

Different channel conditions can produce different types of small-scale fading. The type of fading, experienced by the mobile, depends on the following factors [3.2]:

Multipath propagation. The presence, in the channel, of a reflective surface and objects that cause scattering creates a variation in amplitude, phase, and time delay. The random phase and amplitude of the different multipath components cause fluctuations in the signal strength.

Speed of the mobile. The relative motion between the transmitter and the receiver causes a random frequency modulation, because of the effect of different Doppler shifts on each of the multipath components.

Speed of surrounding objects. The surrounding environment is important in a wireless channel, not only because it changes the multipath components, but also because of varying Doppler shifts for all multipath components.

Bandwidth of the signal. If the transmitted signal bandwidth is greater than the flat-fading bandwidth of the multipath channel, the signal at the receiver antenna is distorted.

The above factors can be reduced to two fundamental causes for small-scale fading:

- time delay spreading of the signal, which can be classified as either flat fading or frequency selective spreading;
- time-variant behaviour of the channel due to the motion of the mobile unit, called Doppler spread.

Time delay signal spread: Flat Fading

Small-scale fading is defined as being *flat* or *non-selective* if the received multipath components of a symbol do not extend beyond the symbol's time duration [3.3].

If the delay of the multipath components with respect to the main component is smaller than the symbol's time duration, a channel is said to be subject to *flat fading*.

In a flat-fading channel inter-symbol interference (ISI) is absent; therefore, such a radio channel has a constant gain and a linear phase response over a bandwidth that is greater than the bandwidth of the transmitted signal (Fig. 25).

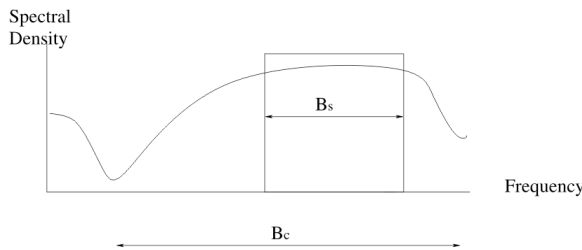


Fig. 25. Flat-Fading case: B_S is the signal bandwidth, and B_C is the coherence bandwidth⁽¹⁾.

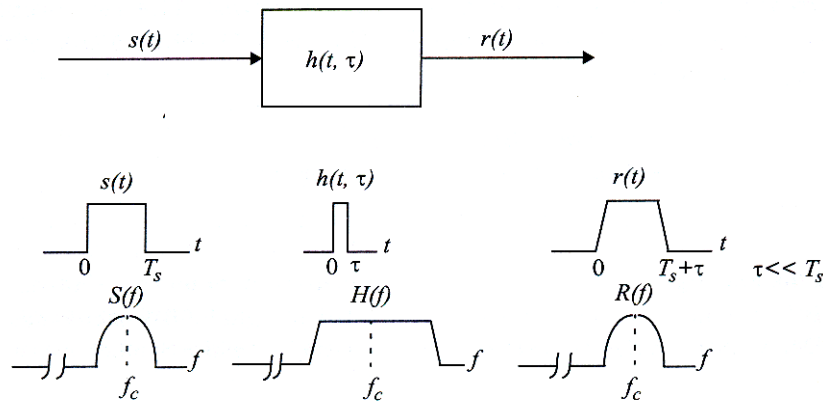


Fig. 26. Flat-Fading channel characteristics⁽⁴⁾.

In a flat-fading channel, the spectral characteristics of the transmitted signal are preserved at the receiver, and the channel does not cause any non-linear distortion due to time dispersion. However, the strength of the received signal generally changes slowly in time, due to the slow gain fluctuations caused by multipath. Flat-fading channels are also known as *amplitude varying channels*, and they are sometimes referred to as *narrowband channels*, as the bandwidth of the applied signal is narrow with respect to the channel bandwidth.

In a flat-fading channel, the following hold true:

$$B_S \ll B_C \quad \text{or} \quad T_S \gg \sigma_\tau \tag{41}$$

where B_S is the bandwidth of the transmitted signal, B_C is the *coherence bandwidth* of the channel, T_S is the symbol's period, and σ_τ is the *rms (root mean square) delay spread* of the channel. These parameters are described in Appendix.

Figure 26 shows the variations in gain of the received signal, while its spectrum is preserved.

Time delay spread: Frequency-Selective Fading

Opposite to the flat fading case previously illustrated, if the channel has a constant gain and a linear phase response over a bandwidth that is much smaller than the bandwidth of the transmitted signal, this channel causes *frequency selective fading* on the received signal [3.3]. Under these conditions, the channel impulse response has a duration greater than the symbol's period. When this occurs, the received signal includes multiple versions of the same symbol, each one attenuated (faded) and delayed. As a consequence, the received signal is distorted, that is, the channel produces inter-symbol interference. In the frequency domain, this means that certain frequency components in the received signal spectrum have larger gains than others (Fig. 27). For frequency selective fading, the spectrum of the received signal has a bandwidth that is greater than the coherence bandwidth B_C . In this case, we say that the channel is frequency-selective.

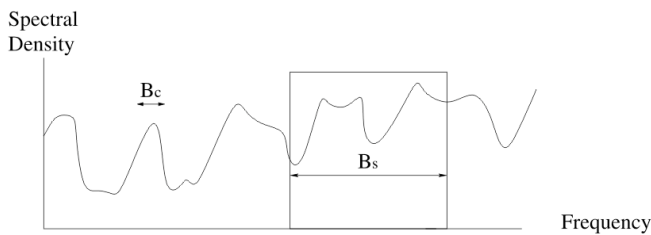


Fig. 27. Frequency-Selective Fading case: B_S is the signal bandwidth, and B_C is the coherence bandwidth⁽¹⁾.

To summarize, a signal undergoes frequency selective fading if

$$B_S > B_C \quad \text{or} \quad T_S < \sigma_\tau \tag{42}$$

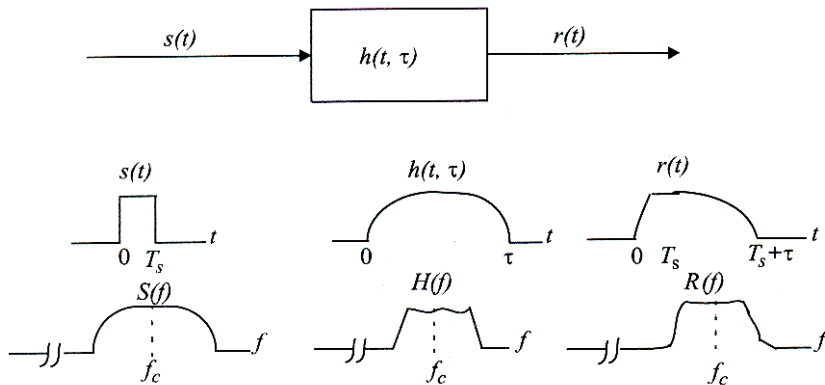


Fig. 28. Frequency-Selective Fading channel characteristics⁽⁴⁾.

Figure 28 illustrates the characteristics of a frequency-selective fading channel. The spectrum $S(f)$ of the transmitted signal has a bandwidth greater than the coherence bandwidth B_C of the channel; in the time domain, the transmitted symbol is shorter than the multipath time delay spread, which causes time dispersion.

Small-scale fading effects due to movements (Doppler Spread)

While the multipath effects described in the previous Section depend on the static geometric characteristics of the environment surrounding the transmitter and the receiver, the Doppler spread is caused by movements in the environment [3.4].

In a *fast fading channel*, the channel impulse response changes rapidly within the symbol duration. The coherence time is a statistical measure of the frequency range where the channel can be considered “flat” [3.2]. If the coherence time is shorter than the symbol duration of the transmitted signal, then the signal undergoes fast fading. In the frequency domain, signal distortion due to fast fading increases with the increasing in the Doppler spread relative to the bandwidth of the transmitted signal. Therefore, the signal undergoes fast fading if

$$T_s > T_C \quad \text{or} \quad B_s < B_D \quad (43)$$

where T_C and B_D are the coherence time and the Doppler bandwidth (i.e. the width of the Doppler power spectrum), respectively (see Appendix). Note that in the case of a frequency-selective, fast fading channel, the amplitude, the phase, and the time delay of each of the multipath components are different for each component.

A classic example of a signal travelling over a fast fading channel was the Morse code signalling, used in the HF frequency band: since the signalling exhibited a very low data rate, its bandwidth was very large, larger than the channel’s coherence bandwidth.

In a *slow-fading channel*, the channel impulse response changes at a rate much slower than the transmitted signal. In this case, the channel can be assumed static over several symbol intervals. In the frequency domain, the Doppler spread is much less than the bandwidth of the signal. To summarize, a signal undergoes slow-fading if

$$T_s \ll T_C \quad \text{or} \quad B_s \gg B_D \quad (44)$$

It is important not to confuse the terms *fast-* and *slow-fading* with the terms *large-scale* and *small-scale fading*. We must emphasize that *fast-* and *slow-fading* deal with the relationship between the time rate of change in the channel and transmitted signal, and not with the propagation path-loss models (*large-scale* or *small-scale* fading).

3.1 Saleh model

Saleh in 1987 reported the results of indoor propagation measurements between two vertically polarized antennas in a medium-sized office [3.5]. The results obtained by Saleh show that the indoor radio channel is very slowly time varying, and that the statistics of the channel’s impulse response are independent of the antenna polarization, if there is no LOS path between transmitter and receiver. Measurements report a maximum delay spread of 100-200 ns within the rooms of a building, and 300 ns in the hallways. The root mean square delay spread inside the rooms has a median of 25 ns and a maximum of 50 ns. With no LOS, the signal attenuation obeys the lognormal law, with an exponent between 3 and 4.

3.2 Rayleigh

The most common characterization of small-scale fading, in a flat-fading mobile radio channel, is by means of the Rayleigh and Ricean models [3.6 – 3.8].

When communications occur in a multi-path environment without LOS, the amplitude of the received signal has typically a Rayleigh distribution. The Rayleigh distribution has a probability density function given by:

$$p(r) = \frac{r e^{-\left(\frac{r^2}{2\sigma^2}\right)}}{\sigma^2} \quad 0 \leq r \leq \infty \quad (45)$$

where σ^2 is the variance of the received signal r .

Two important statistics exist for determining error control codes and diversity schemes to be used in a communication system: the *level crossing rate* (LCR) and the *average fade duration* (AFD), respectively. The received signal in mobile radio communications often undergoes heavy statistical fluctuations; in digital communications, a heavy decline of the received signal directly leads to a drastic increase in the bit error rate. For optimizing coding systems, which are required for error correction, it is important not only to know how often the received signal

crosses a given threshold R , but also for how long time, on average, the signal is below a certain level. Suitable measures for characterizing this process are the LCR and the AFD.

The number of level crossings per second is given by

$$N_R = \sqrt{2\pi} f_{\max} \rho e^{-\rho^2} \quad (46)$$

where f_{\max} is the maximum Doppler frequency, and $\rho = R/R_{rms}$ is the value of the specified signal level R normalized to the local root mean square amplitude of the fading envelope. AFD is defined as the mean time period during which the receiver signal is below a specified level R ; it depends on the speed of the mobile and is given by

$$AFD = \bar{\tau} = \frac{e^{\rho^2} - 1}{\rho f_{\max} \sqrt{2\pi}} \quad (47)$$

Another mode to view the Rayleigh distribution is as the probability density function of the receiver signal amplitude to the noise ratio, which is proportional to the square of the signal envelope. Let A be the receiver signal-to-noise ratio; the probability density function of A is exponential [3.9] and can be written as

$$p_A(a) = \frac{1}{\rho} \exp\left(-\frac{a}{\rho}\right) \quad a \geq 0 \quad (48)$$

where $\rho = E[A]$. The LCR can be written as

$$N_R(a) = \sqrt{\frac{2\pi a}{\rho}} f_{\max} \exp\left(-\frac{a}{\rho}\right) \quad \text{or} \quad N_R(a) = \sqrt{2\pi a \rho} f_{\max} p_A(a) \quad (49)$$

3.3 Ricean

When a LOS propagation path does exist, there is a dominant signal component; in this case the small-scale fading distribution obeys the Ricean one. At the receiver, the signal appears as a continuous component added with a random multi-path component. The Ricean distribution is given by

$$p(r) = \frac{r}{\sigma^2} \exp\left(-\frac{r^2 + A^2}{2\sigma^2}\right) I_0\left(\frac{Ar}{\sigma^2}\right), \quad r \geq 0 \quad (50)$$

where A denotes the peak amplitude of the dominant signal and $I_0(\cdot)$ is the modified Bessel function of the first kind and zero order. The Ricean distribution is often described in terms of a parameter K , which is the ratio between the deterministic signal power and the variance of the multi-path component:

$$K = \frac{A^2}{2\sigma^2} \quad (51)$$

The parameter K completely specifies the Ricean distribution. For $K = 0$ the Ricean distribution reduces to a Rayleigh distribution. The LCR for a Ricean distribution is given by

$$N_a = \sqrt{\frac{\beta}{2\pi}} p(r) \quad (52)$$

where $\beta = 2(\pi\sigma f_{\max})^2$, and σ^2 is the variance of the received signal.

The calculation of the probability density function of fading intervals, carried out by Rice [3.10], caused various additional research activities in this field [3.11 – 3.14]. The mathematical treatment of the so-called *level-crossing problem* is extremely difficult, also for Rayleigh channels, and a satisfactory general solution is still to be found. Special attention in this field should be given to the works carried out by D. Wolf in [3.15 – 3.19]

IV. Current Outdoor Measurements

The Wireless Networks Laboratory at CNR-ISTI started in 2005 a wide measurement campaign on packet losses over WLANs with the aim of coming to defining wireless channel indoor and outdoor models more suitable than those available in the literature. The measurement campaign is still in progress. A first set of preliminary measurements of packet losses and power levels has just been completed, in outdoors environments, by using the built-in signal level monitor available in the wireless boards. The measurements have been carried out in a rural environment, such as a wide field not cultivated, without interferences due to other wireless networks, and without reflections due to walls, trees, lampposts or buildings. Some applications can be used in this type of environments; for instance, precision agriculture is one of the promising domains where wireless sensor networks could be exploited, by observing the microclimate within a field, so that plant-specific farming can ultimately be realized. In this context, the wireless networks can be used to create a backbone between sensor networks and terrestrial networks.

Statistics about packet losses and power levels of all received packets at various distances between transmitter and receiver and various bit rates have been collected, once fixed the transmitter and receiver height from ground (90 cm), and the antenna's orientation (LOS orientation). Packets were generated by using a proprietary C program, ad-hoc written for this purpose. The traffic was of CBR (Constant Bit Rate) type, generated at 1.6 Mbps when the bit rates were 11, 5.5 and 2Mbps, and at 800Kbps when the bit rate was 1Mbps. The mobile devices used are IBM Thinkpad R40e laptops (Celeron 2.0 GHz with 256 Mb Ram running Debian Linux with a 2.6.8 kernel), equipped with CNet CNWLC-811 IEEE 802.11b wireless cards. Transmitter and receiver nodes have been set up in ad-hoc mode, with retry limit set to zero.

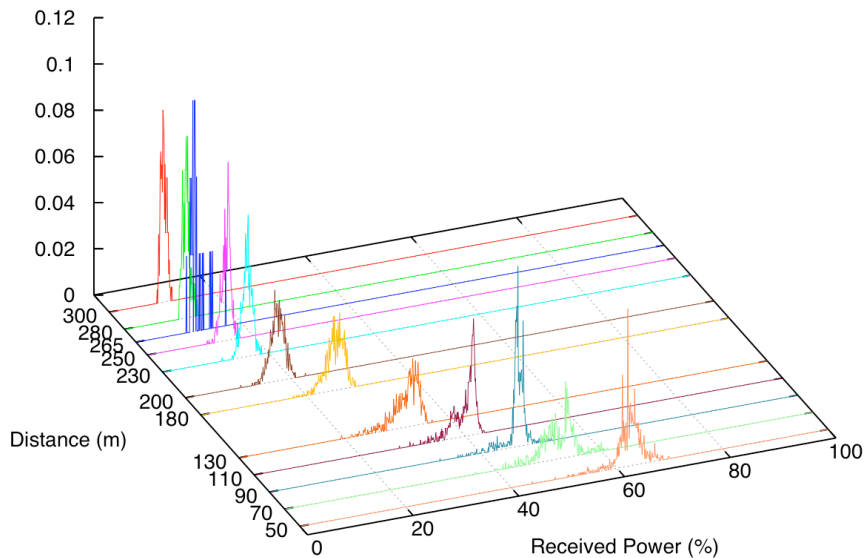


Fig. 29. Probability Density Function of the received signal versus the distance between transmitter and receiver.

Figure 29 shows the Probability Density Function (PDF) of the received power for different distances, with a bit rate set to 11Mbps. As expected, we measured that the signal level decreases with the increase in distance between transmitter and receiver; in fact, we measured a signal level equal to 65, in a [0 – 100] range, when the distance was 50 m and we reached only a signal level equal to 15 when the distance was 200 m. By using the other bit rates we obtained a similar behavior of the signal level versus distance. This behavior is reported in Fig. 30, where minimum, maximum and mean values of the signal level PDF are shown. The maximum and minimum values are taken as the 95th and 5th percentiles of the PDF, respectively. There are

two aspects to point out: *i)* by fixing the bit rate, these three curves are very close together, and *ii)* the tendency of the signal level is independent of the bit rates.

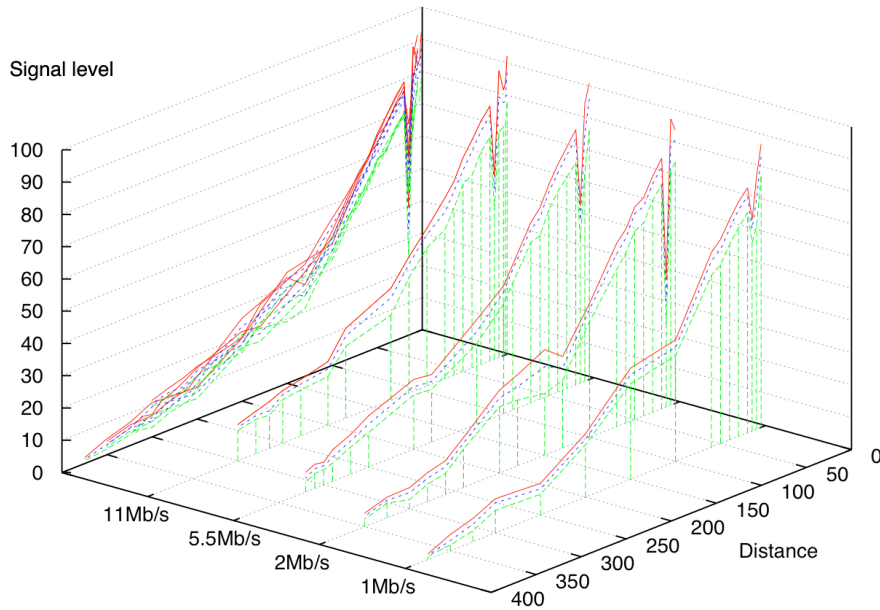


Fig. 30. Maximum, minimum and mean value of the received power versus distance, for all four speeds.

Measurements show that the 2-Ray model well suits this rural environment (Fig. 31). The solid red line represents the theoretical 2-Ray model (with reflection coefficient = -1), while the vertical blue lines represent the minimum, maximum and mean values of the signal level at different distances between transmitter and receiver. These values have been normalized to the signal level value obtained when the distance between transmitter and receiver is 1 m.

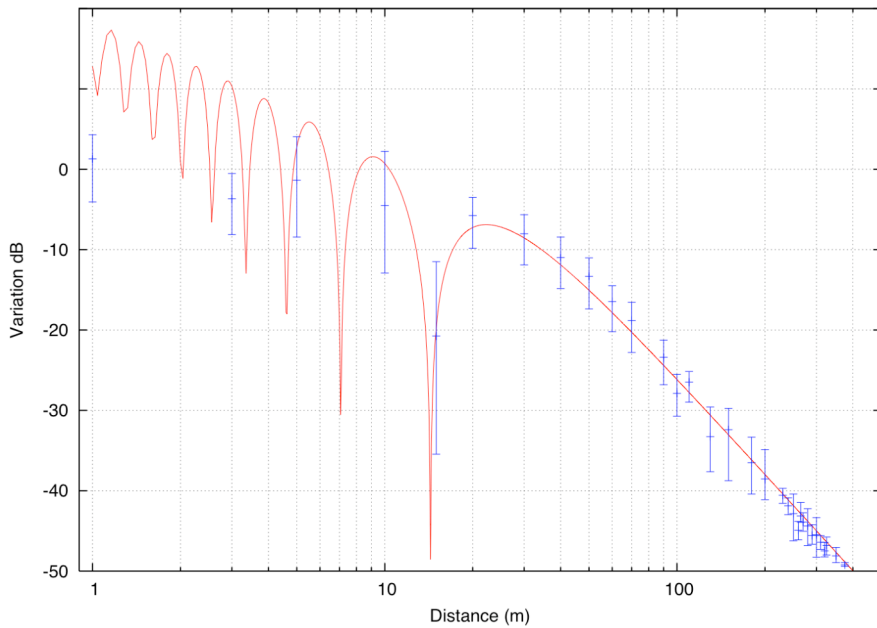


Fig. 31. Comparison between 2-Ray model and power measurements.

As we can see in Fig. 31, for distances shorter than the first Fresnel zone ($d_F = 4h_t h_r / \lambda \approx 31$ m), the power of the received signal drops down at about -10dB/decade; instead, for distances

greater than the first Fresnel zone, the power drops down at about -40dB/decade. Note that at a distance of 15 m between receiver and transmitter, the power abruptly falls down at about -20 dB because the wireless cards are sensitive to the disruptive interference at 15 m due to the 2-Ray model.

Finally, we tried to find a connection between the received power levels and the relevant packet losses. Figure 32 clearly shows the threshold effect at a distance between transmitter and receiver of about 200 m for measures carried on at 11Mbps; in fact, within this distance, the packet loss is practically zero, while the packet loss rapidly increases, beyond this distance.

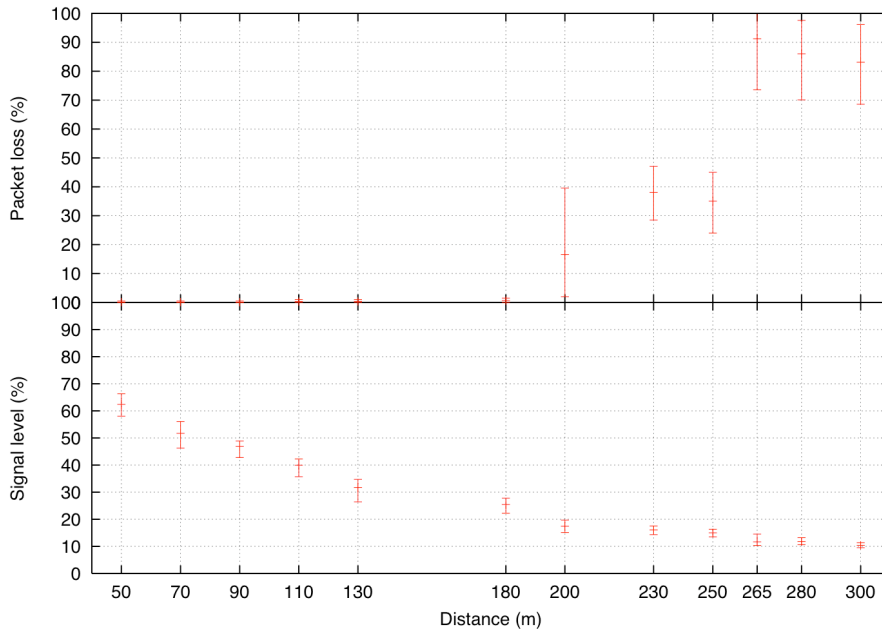


Fig. 32. Comparison between packet loss and signal level versus distance.

Table XI summarizes the packet loss threshold, the signal level threshold and the differences between these two types of thresholds for different values of bit rates.

Table XI. Packet loss threshold for different bit rates

Bit rate	Packet loss threshold	Signal level threshold	Δ (m)	Δ (%)
11 Mbps	180 m/200 m	18%		
5.5 Mbps	250 m/270 m	13%	+70 m	-5%
2 Mbps	260 m/280 m	10%	+10 m	-3%
1 Mbps	325 m/350 m	5%	+70 m	-5%

As we can see from Table XI, when the bit rate decreases in the range 11 Mbps–1 Mbps (column one), the gain, in terms of distance between transmitter and receiver, increases by 70, 10 and 70 meters, respectively, while the signal level decreases by 5%, 3% and 5%, respectively.

In conclusion, our measurements confirm that the received power is independent of the bit rates and that the 2-Ray model well suits a rural environment.

V. Conclusions

This tutorial, other than giving an overview of the most popular channel models for terrestrial wireless communications, tries to summarize how to recognize which types of fading the signal

undergoes in a terrestrial wireless environment. For instance, the IEEE802.11 standard specifies which physical layer must be used in Wireless LAN in the 2.4 GHz Industrial-Scientific-Medical band, and it fixes the symbol period length ($T_s \approx 90$ ns) [5.1 – 5.4]. In Table XII different types of *delay spread* for indoor radio channels are shown.

By looking at these values it is possible to deduce that the channel is *flat* when the *delay spread* is greater than the symbol period ($T_s > \sigma_\tau$).

As the value of the coherence time is estimated, by calculating the maximum Doppler frequency, we can choose the speed of the mobile nodes, for example 100 Km/h and 2 m/s. With these values of speed, the maximum shift frequency is given by

$$f_{\max} = \frac{v}{c_0} f_0 = \begin{cases} 224 \text{ Hz} & (100\text{Km/h}) \\ 16 \text{ Hz} & (2\text{m/s}) \end{cases}$$

and the coherence time, which is inversely proportional to the Doppler spread, is given by

$$T_C \approx \frac{1}{f_{\max}} = \begin{cases} 4.46\text{ms} \\ 62.5\text{ms} \end{cases}$$

Since the coherence time is much greater than the symbol period ($T_s \ll T_C$), this is a slow-fading channel. Similar considerations can be done for the IEEE802.11g standard, where the symbol's period T_s is 4 μ s; in this case the channel is flat and the fading is slow.

Table XII. Typical values of mean and maximum delay spread

Mean delay spread [ns]	Maximum delay spread [ns]	Reference	Remarks
40	120	[A.2]	Large building
40	95	[A.3]	Office building
40	150	[A.4]	Office building
60	200	[A.5]	Shopping center
106	270		Laboratory
19	30	[A.6]	Office building: single room only
20	65	[A.7]	Office building
30	75		Canteen
105	170		Shopping center
30	56	[A.8]	Office building
25	30	[A.9]	Office building: single room only

Figure 33 summarizes the types of channels based on a classification of small-scale fading.

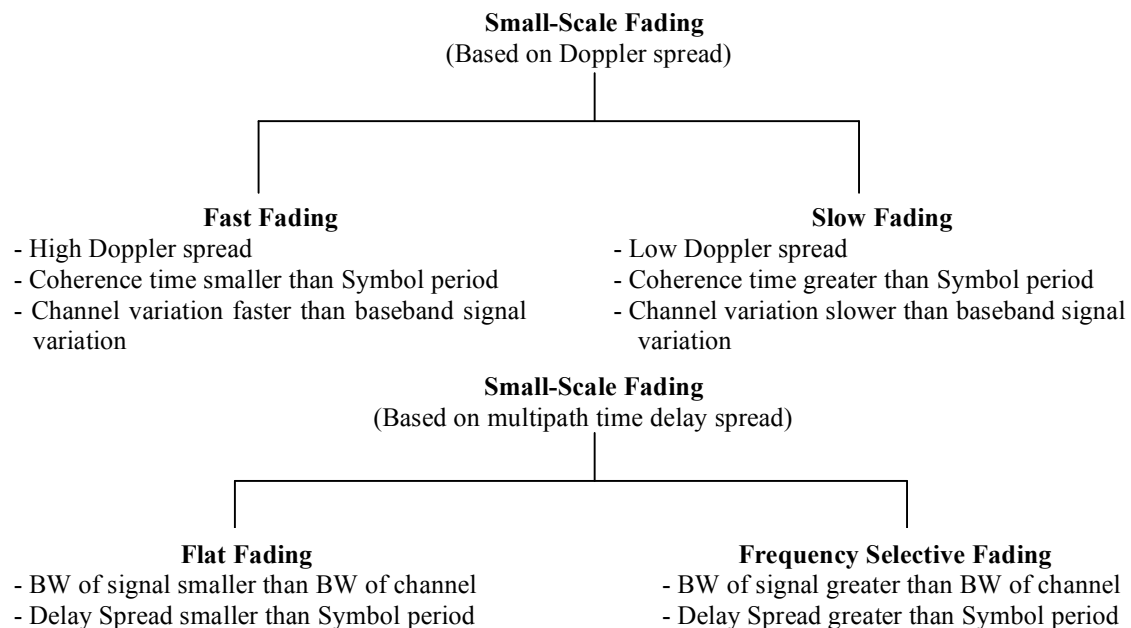
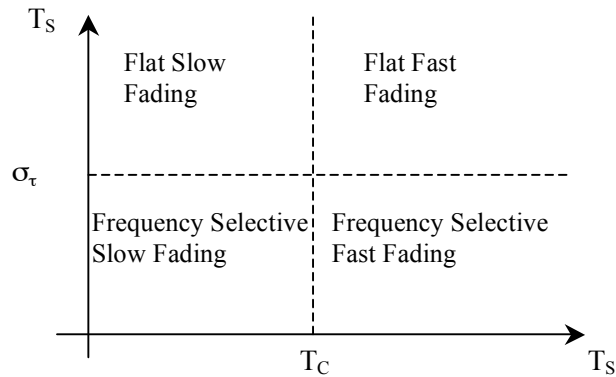
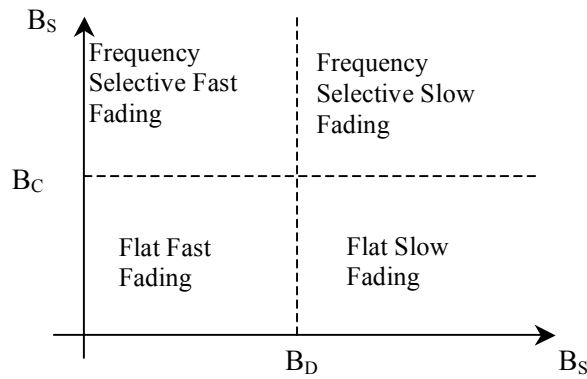


Fig. 33. Types of small-scale fading (BW stands for “bandwidth”)

The relationships among the various multipath parameters and the types of fading experienced by the signal are summarized in Fig. 34, where four regions are distinguished.



(a) Time domain



(b) Frequency domain

Fig. 34. Small-scale fading types experienced by a signal from the viewpoint of (a) symbol period, (b) base-band signal bandwidth.

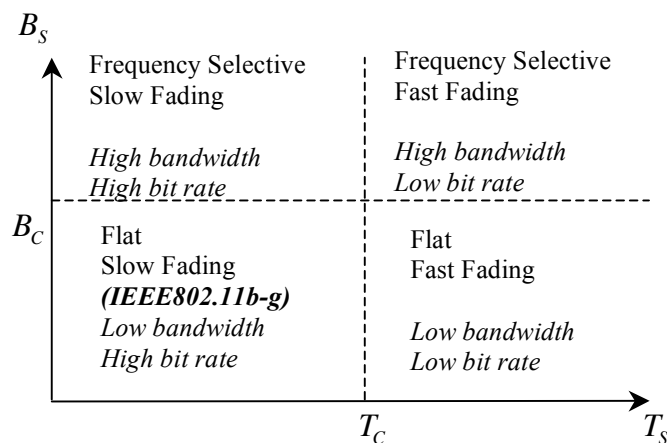


Fig. 35. Small-scale fading types for the IEEE802.11 signal.

Finally, Fig. 35 summarizes the types of the small-scale fading for the IEEE 802.11 signal. For high bandwidth relative to the coherence bandwidth, the transmitted signal undergoes frequency-selective, while for low bit rate relative to the coherence time the signal undergoes fast-fading.

Acknowledgements

The author warmly thanks Dr. Nedo Celandroni, Dr. Erina Ferro, and Dr. Francesco Potorti for their precious suggestions and support in preparing this work.

References

- [1.1] Cox, D.C., "Cochannel Interference Considerations in Frequency Reuse Small-Coverage Area Radio System," IEEE Trans. on Comm., Vol. COM-30, No. 1, Jan. 1982, pp. 135-142.
- [1.2] K. Daikoku and H. Ohdate, "Optimal channel reuse in cellular land mobile radio systems," IEEE Trans. Veh. Technol., vol. VT-32, pp. 217-224, Aug. 1983.
- [1.3] D.J. Goodman, R.A. Valenzuela, K.T. Gayliard and B. Ramamurthi, "Packet Reservation Multiple Access for Local Wireless Communications", In proceedings of the IEEE 38 th Vehicular Technology Conference, Philadelphia, PA, USA, pp. 701-706, June 1988.
- [1.4] D.J. Goodman, R.A. Valenzuela, K.T. Gayliard and B. Ramamurthi, "Packet Reservation Multiple Access for Local Wireless Communications", IEEE Transactions on Communications, Vol. 37, Issue 8, pp. 885-890, August 1989.
- [1.5] Hafez, H.M., and G.H. Nehme, "Data Transmission Over Cellular Radio System Using a Single Radio Frequency," Proc. Eurocom, Stockholm, June 1988, pp. 367-370.
- [1.6] Wilson, N.D., and S.S. Rappaport, "Cellular Mobile Packet Radio Using Multiple-Channel CSMA," IEEE Proc. F (GB), Vol. 132, No. 6, Oct. 1985, pp. 517-526.
- [1.7] Oeting, J., "Cellular Mobile Radio – An Emerging Techonology," IEEE Communications Magazine, pp. 10-15, November 1983.
- [1.8] MacDonald, V.H., "The Cellular Concept," The Bell Systems Technical Journal, Vol. 58, No. 1, pp. 15-43, January 1979.
- [1.9] Rappaport, T.S., "Wireless Communications", Prentice-Hall, Upper Saddle River, New Jersey, Ch. 3 and 4, 1996.
- [1.10] Jakes, W.C., Ed., "Microwave Mobile Communications. Piscataway", New York: IEEE Press, 1993.
- [1.11] W. C. Jakes, Jr., Microwave Mobile Communications. New York: Wiley, 1974.
- [1.12] Oppenheim A.V. and Schafer R.W., Digital Signal Processing. Englewood Cliffs, New Jersey: Prentice-Hall, 1975.
- [1.13] W. C. Jakes, Jr., Microwave Mobile Communications. New York: John Wiley and Sons, 1978.
- [1.14] Lee, W.C.Y., Mobile Communications Design Fundamentals, Indianapolis: Howard W. Sams & Co., 1986.
- [1.15] Parson D., The Mobile Radio Propagation Channel, New York: Halsted Press (John Wiley & Sons, Inc.), 1992.
- [1.16] Lee, W.C.Y., "Elements of cellular mobile radio system, IEEE Trans. Vehicular Technol., V-35(2), 48-56, May 1986.

- [2.1] Sklar, B., Digital Communications: Fundaments and Applications, 2th ed., *Prentice-Hall, Englewood Cliffs*, NJ, Ch. 4, 2001.
- [2.2] Sklar, B., "Rayleigh fading channels in mobile digital communication systems" IEEE Communications Magazine, Volume 35, Issue 7, July 1997 Page(s):90 - 100
- [2.3] J.P. Linnartz., Narrowband Land-Mobile Radio Networks, *Artech house*, 1993
- [2.4] Dai Lu and Dave Rutledge, "Investigation of indoor radio channels from 2.4GHz to 24GHz", IEEE Antennas and Propagation Symposium (APS/URSI) , pp. 134-137, June, 2003, Columbus OH.
- [2.5] Cox, D.C., Murray, R., and Norris, A., "800MHz Attenuation measured in and around suburban houses", Bell Laboratory Technical Journal, 673(6), 921-954, Jul.-Aug. 1984.
- [2.6] Gibson, J.D., "The Mobile Communications Handbook", 2th ed. *CRC Press* 2002.
- [2.7] Scott Y. Seidel, Theodore S. Rappaport, Sanjiv Jain, Michael L. Lord, Rajendra Singh, "Path Loss, Scattering, and Multipath Delay Statistics in Four European Cities for Digital Cellular and Microcellular Radiotelephone", IEEE Transactions on vehicular technology, Vol 40, No. 4, pp. 721 – 730, November 1991.
- [2.8] Von Hippel, A.R., "Dielectric Materials and Applications", Publication of MIT Press, MA, 1954.
- [2.9] Rappaport, T.S., "Wireless Communications", Prentice-Hall, 2th ed. Upper Saddle River, New Jersey, 2002.

- [2.10] Feuerstein, M. J., Blackard, K. L., Rappaport, T. S., Seidel, S. Y., and Xia, H. H., "Path loss delay spread and outage models as functions of antenna height for microcellular system design," *IEEE Transactions on Vehicular Technology*, Vol. 43, No. 3, pp. 487-498, August 1994.
- [2.11] R. Wolfson and J. M. Pasachoff., "Physics with Modern Physics", Harper Collins College Publishers, New York, NY USA, 1995.
- [2.12] E. Hecht., "Optics", Pearson Education Inc., San Francisco, CA. USA, fourth edition, 2002.
- [2.13] Lee, W. C. Y., "Mobile Communications Engineering", McGraw Hill Publication, New York, 1985.
- [2.14] Bullington K., "Radio Propagation at Frequencies Above 30 Megacycles," *Proc. of the I.R.E.*, vol. 35, pp.1122-1136, Oct 1947.
- [2.15] Deygout J., "Multiple Knife-Edge Diffraction of Microwaves," *IEEE Trans. Ant. Prop.* vol. AP-14, no. 4, pp. 480-489, July 1966.
- [2.16] Epstein J, Peterson D W, "An Experimental Study of Wave Propagation at 850 MC", *Proc. of the I.R.E.*, vol. 41, pp. 595-611, May 1953.
- [2.17] Leberherz, M, et.al. "A versatile wave propagation model for the VHF/UHF range considering three-dimensional terrain." *IEEE Trans. on Ant. and Prop.* 40(10), pp. 1121-1131, Oct. 1992.
- [2.18] Tameh, E K, et.al. "A 3-D integrated macro and microcellular propagation model, based on the use of photogrammetric terrain and building data," In *Proceedings of IEEE VTC'97*, vol. 3, 1997, pp. 1957-1961, Phoenix, USA, 1997
- [2.19] Van Rees, J., "Measurements of the Wideband Radio Channel Characteristics for Rural, Residential and Suburban areas", *IEEE Transactions on Vehicular Technology*, Vol. VT-36, pp.1-6, February 1987.
- [2.20] Zogg, A., "Multipath Delay Spread in a Hilly Region at 210 MHz", *IEEE Transactions on Vehicular Technology*, Vol. VT-36, pp.184-187, November 1987.
- [2.21] Seidel, S.Y., Rappaport, T.S., Jain, S., Lord, M., and Singh, R., "Path Loss, Scattering and Multipath Delay Statistics in Four European Cities For Digital Cellular and Microcellular Radiotelephone," *IEEE Transactions on Vehicular Technology*, Vol. 40, No. 4, pp.721-730, November 1991.
- [2.22] Rice, P.L., Longley, A. G., Norton, K. A., and Baris, A. P., "Transmission loss predictions for tropospheric communication circuits" *NBS Tech Note 101*; two volumes; issued May 7, 1965; revised May 1, 1966; revised January 1967
- [2.23] Longley, A. G., and Rice, P.L., "Prediction of tropospheric radio transmission loss over irregular terrain; A computer method" *ESSA Technical Report*, ERL 79-ITS 67, 1968
- [2.24] Longley, A. G., "Radio propagation in Urban Areas" *OT Reort*, pp. 78-144, April 1978
- [2.25] Okumura, T., Ohmori, E., and Fukuda, K., "Field strength and its variability in VHF and UHF land mobile service" *Review electrical communication laboratory*, vol. 16, No. 9-10, pp. 825-873, September-october 1968.
- [2.26] Y. Okumura, E. Ohmori, T. Kawano, K. Fukuda. "Field strength and its variability in VHF and UHF land-mobile service." *Review of the Electrical Communications Laboratory*, Vol. 16, pp. 825-873, September 1968.
- [2.27] M. Hata. "Empirical formula for propagation loss in land mobile radio services." *IEEE Transactions on vehicular technology*, Vol. 29, pp.317-325, 1980.
- [2.28] European cooperation in the field of scientific and technical research EURO-COST 231, "Urban transmission loss models for mobile radio in the 900 and 1800 MHz bands" revision 2, The Hague, September 1991.
- [2.29] Walfisch, J., and Bertoni, H. L., "A theoretical model of UHF propagation in urban environments" *IEEE transactions on antennas and propagation*, Vol. AP-36, pp. 1788-1796, October, 1988.
- [2.30] Xia, H., and Bertoni, H. L. "Diffraction of cylindrical and plane waves by an array of absorbing half screens" *IEE transactions on antennas and propagation*, Vol. 40, No. 2, pp. 170-177, February 1992.
- [2.31] Maciel, L. R., Bertoni, H. L., and Xia, H. H., "Unified approach to prediction of propagation over buildings for all ranges of base station antenna height" *IEEE transactions on vehicular technology*, Vol. 42, No. 1, pp. 41-45, February 1993.
- [2.32] Recommendation M.1455: "Key characteristics for the international mobile telecommunications 2000 (IMT-2000) RADIO INTERFACES"
- [2.33] Recommendation M.1225: "Guidelines for evaluation of radio transmission technologies for IMT-2000".

- [2.34] Cox, D.C., Murray, R. R., and Norris, A.W., "Measurements of 800MHz radio transmission into buildings with metallic walls" *Bell System technical journal*, Vol. 62, No. 9, pp. 2695 – 2717, November 1983.
- [2.35] Alexander, S. T., "Radio propagation within buildings at 900 MHz" *Electronics letters*, Vol. 18, No. 21, pp. 913-914, 1982.
- [2.36] Molkdar, D., "Review on radio propagation into and within buildings" *IEEE Proceedings*, Vol. 138, No. 1, pp. 61-73, February 1991.
- [2.37] Hashemi, H., "The indoor radio propagation channel" *Proceedings of the IEEE*, Vol. 81, No. 7, pp. 943-968, July 1993.
- [2.38] Seidel, S.Y., et.al., "The impact of surrounding buildings on propagation for wireless inbuilding personal communications system design", *IEEE Vehicular technology conference*, Denver, ,pp. 814-818, May 1992.
- [2.39] Seidel, S.Y., and Rappaport, T.S., "914 MHz path loss prediction models for indoor wireless communications in multifloored buildings" *IEEE Transaction on antenna and propagation*, Vol. 40, No. 2, pp. 207-217, February 1992.
- [2.40] Rappaport, T.S., "Characterization of UHF Multipath radio channels in factory buildings" *IEEE Transactions on antenna and propagation*, Vol. 37, No. 8, pp. 1058-1069, August 1989.
- [2.41] Andersen, J.B., Rappaport, T.S., and Yoshida, S., "Propagation measurements and models wireless communications channels" *IEEE Communications magazine*, Vol. 33, No 1, pp. 42 - 49, 1994. November 1994.
- [2.42] Devasirvatham, D.M.J., Banerjee, C., Krain, M.J., and Rappaport, D.A., "Multi-frequency radiowave propagation measurements in the portable radio environment" *IEEE International conference on communications*, pp. 1334-1340, 1990.
- [2.43] Rappaport, T. S., "The Wireless Revolution" *IEEE Communications Magazine*, pp. 52-71, November 1991.
- [2.44] Violette, E. J., Espeland, R. H., and Allen, K. C., "Millimeter-Wave Propagation characteristics and channel performance for Urban-Suburban environments" *National Telecommunications and Information Administration*, NTIA Report 88-239, December 1988.
- [2.45] Bernhard H. Walke "Mobile Radio Networks" *John Wiley & Sons*, 2002
- [2.46] H. H. Xia, H. L. Bertoni, L. R. Maciel, A. Lindsay-Stewart, and R. Rowe, "Radio propagation characteristics for line-of-sight microcellular and personal communication," *IEEE Trans. Antennas Propagat.*, vol. 41 pp. 1439-1447, Oct. 1993.
- [3.1] Boithias, L., "Radio Wave Propagation", *McGraw-Hill*, New York 1987.
- [3.2] Gibson, J.D., "The Mobile Communications Handbook", *CRC Press* 1996.
- [3.3] Amoroso, F., "The Bandwidth of Digital Data Signals," *IEEE Communications Magazine*, vol. 18, no. 6, November 1980, pp. 13-24.
- [3.4] Clarke, R.H., "A statistical theory of mobile radio reception", *Bell Syst. Tech. J.*, 47(6), 957-1000, Jul.-Aug. 1968.
- [3.5] Saleh, A.A.M., and Valenzuela, R.A., "A statistical model for indoor multipath propagation" *IEEE Journal an selected areas in communication*, Vol. JSAC-5, No.2, pp. 128-137, February 1987.
- [3.6] Young W.R., "Comparison of Mobile Radio Transmission at 150, 450, 900 and 3700MHz," *Bell Syst. Tech. J.*, Vol. 31, pp. 1068-1085, Nov. 1952.
- [3.7] Hulund H.W., "Characteristics of Small-area Signal Fading on Mobile Circuits in the 150 MHz Band," *IEEE Trans. Veh. Technol.*, Vol. 17, pp.24-30, Oct. 1968.
- [3.8] Okumura Y. Ohmori E. Kawano T, and Fukuda K., "Field strength and its variability in VHF and UHF land mobile radio services," *Rev. Elec. Commun. Lab.*, Vol. 16 pp. 825-873, Sep./Oct. 1968.
- [3.9] J. G. Proakis, "Digital Communications", 2° ed. McGraw-Hill New York, 1989.
- [3.10] Rice S.O. "Disribution of the duration of fades in radio transmission: Gaussian noise model," *Bell Syst. Tech. J.*, Vol 37, pp. 581-635, May 1958.
- [3.11] McFadden J.A., "The axis-crossing intervals of random functions II," *Trans. Inst. Rad. Eng.*, Vol. 4, pp. 14-24, 1958.
- [3.12] McFadden J.A., "The axis-crossing intervals of random functions I," *Trans. Inst. Rad. Eng.*, Vol. 2, pp. 146-150, 1956.
- [3.13] Longuet-Higgings M.S., "The distribution of intervals between zeros of a stationary random function," *Phil. Trans. Royal. Soc.*, Vol. A 254, pp. 557-599, 1962.
- [3.14] Rainal A.J., "Axis-crossing intervals of Rayleigh processes," *Bell Syst. Tech. J.*, Vol 44, pp, 1219-1224, 1965.

- [3.15] Munakata T. and Wolf D., "A novel approach to the level-crossing problem of random processes," in Proc. of the 1982 IEEE Int. Symp. on Inf. Theory, Les Arcs, France, 1982, Vol. IEEE-Cat. 82 CH 1767-3 IT, pp. 149-150.
- [3.16] Munakata T. and Wolf D., "On the distribution of the level-crossing time-intervals of the random processes" in Proc. of the 7th Int. Conf. on Noise in Physical System, Montpellier, USA, M. Savelli, G. Lecoy, and J.P. Nougier, Eds., North-Holland Publ. Co., Amsterdam, The Netherlands, 1983, pp. 49-52.
- [3.17] Wolf D. Munkata T. and Wehhofer J., "Die Verteilungsdichte der Pegelunterschreitungszeitintervalle bei Rayleigh_Fadingkanalen." NTG-Fachberichte 84, pp. 23-32, 1983.
- [3.18] Wolf D. Munkata T. and Wehhofer J., "Statistical properties of Rice fading processes," in Signal Processing II: Theories and Applications, Proc. EUSIPCO'83 Second European Signal Processing Conference, H.M. Schubler, Erlangen, Ed., Elsevier Science Publishers B.V. (North-Holland), 1983, pp. 17-20.
- [3.19] Tezlaff, R. Wehhofer J. and Wolf D., "Simulation and analysis of Rayleigh fading processes," in Proc. of the 9th Int. Conf. on Noise in Physical Systems, Montreal, Canada, 1987, pp. 113-116.
- [5.1] ISO/IEC 8802-11; ANSI/IEEE Std 802.11, 1999 edn Information technology - telecommunications and information exchange between systems - local and metropolitan area networks - specific requirements. Part 11: wireless LAN Medium Access Control (MAC) and Physical Layer (PHY) specifications.
- [5.2] ISO/IEC 8802-11:1999/Amd 1:2000(E); IEEE Std 802.11a-1999 Information technology-telecommunications and information exchange between systems- local and metropolitan area networks- specific requirements part 11: wireless LAN medium access control (MAC) and physical layer (PHY) specifications amendment 1: high-speed physical layer in the 5 GHz band.
- [5.3] IEEE Std 802.11b-1999 Supplement To IEEE Standard For Information Technology-Telecommunications And Information Exchange Between Systems- Local And Metropolitan Area Networks- Specific Requirements- Part 11: Wireless LAN Medium Access Control (MAC) And Physical Layer (PHY) Specifications: Higher-speed Physical Layer Extension In The 2.4 GHz Band.
- [5.4] IEEE Std 802.11g-2003 Amendment to IEEE Std 802.11, 1999 Edn. (Reaff 2003) as amended by IEEE Stds 802.11a-1999, 802.11b.
- [A.1] Lee, W.C.Y., "Mobile Cellular Telecommunications System," McGraw Hill Publications, New York, 1989
- [A.2] D.M.J. Devasirvatham, "Multi-Frequency Propagation Measurements and Models in a Large Metropolitan Commercial Building for Personal Communications," IEEE PIMRC '91, September 23-25, London, pp. 98-103.
- [A.3] D.M.J. Devasirvatham, "Time Delay Spread Measurements at 850 MHz and 1.7 GHz inside a Metropolitan Office Building," Electronics Letters, February 2, 1989, pp. 194-196.
- [A.4] D.M.J. Devasirvatham, M.J. Krain and D.A. Rappaport, "Radio Propagation Measurements at 850 MHz, 1.7 GHz and 4 GHz inside two dissimilar office buildings," Electronics Letters, vol. 26, no. 7, March 29, 1990, pp. 445-447.
- [A.5] I.T. Johnson and E. Gurdenelli, "Measurements of Wideband Channel Characteristics in Cells Within Man Made Structures of Area Less Than 0.2 km", COST 231 TD(90)083.
- [A.6] J. Lahteenmaki, "Indoor Measurements and Simulation of Propagation at 1.7 GHz," COST 231 TD(90)084.
- [A.7] P.C. Anderson, O.J.M. Houen, K. Kladakis, K.T. Peterson, H. Fredskild and I. Zarnoczay, "Delay Spread Measurements at 2 GHz", COST 231 TD(91)029.
- [A.8] R.J.C. Bultitude, S.A. Mahmoud and W.A. Sullivan, "A Comparison of Indoor Radio Propagation Characteristics at 910 MHz and 1.75 GHz", IEEE Journal on Selected Areas in Communications, vol. 7, No. 1, January 1989, pp. 20-30.
- [A.9] P. Nobles and F. Halsall, "Delay Spread and Received Power Measurements Within a Building at 2 GHz, 5 GHz and 17 GHz," IEEE Tenth International Conference on Antennas and Propagation, Edinburgh, No 436, pp. 2319-2324, April 14-17, 1997.
- [A.10] Steele, R., "Mobile Radio communications", ed. IEEE Press, 1994.
- [A.11] Bogusch, R.L., "Digital communications in fading channels: Modulation and coding" Mission Research Corp., Santa Barbara, California, Report No. MRC-R-1043, Mar. 11, 1987.

Appendix

Time dispersion

The *mean excess delay*, the *rms (root mean square) delay spread*, and the *maximum excess delay spread* are parameters that can be calculated from the power profile. The *mean excess delay* is the first moment of the power delay profile, and is defined as [A.1]

$$\tau = \frac{\sum_k a_k^2 \tau_k}{\sum_k a_k^2} = \frac{\sum_k P(\tau_k) \tau_k}{\sum_k P(\tau_k)} \quad (\text{A.1})$$

where a_k is the amplitude of the k th-component that arrives at the receiver, and $P(\tau_k)$ is the power of the k th-component. The *rms delay spread* is the square root of the second moment of the power delay profile; it is defined as

$$\sigma_\tau = \sqrt{\bar{\tau}^2 - (\bar{\tau})^2} \quad (\text{A.2})$$

where

$$\bar{\tau}^2 = \frac{\sum_k a_k^2 \tau_k^2}{\sum_k a_k^2} = \frac{\sum_k P(\tau_k) \tau_k^2}{\sum_k P(\tau_k)} \quad (\text{A.3})$$

Typical values of delay spread are shown in Table XII, which shows different values for indoor radio channels.

The *maximum excess delay* (MED) is defined as the time delay during which the multipath energy falls to a certain number of dBs below the maximum (Fig. A.1).

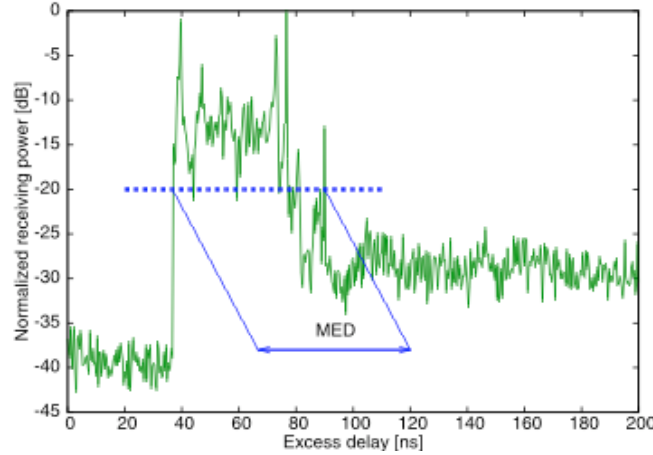


Fig. A.1. Maximum excess delay (where the threshold is fixed to -20 dB).

It is important to underline that the values $\bar{\tau}$, $\bar{\tau}^2$, and σ_τ depend on the choice of the *noise threshold*. The *noise threshold* is the threshold used to differentiate the noise from the received multipath components. If the noise threshold is set too low, the noise is seen like a multipath component, and $\bar{\tau}$, $\bar{\tau}^2$, and σ_τ increase.

Coherence bandwidth

Analogously to the *delay spread* parameters in the time domain, the *coherence bandwidth* B_C is used to characterize the channel in the frequency domain. The *coherence bandwidth* is a statistical measure of the frequency range where the channel can be considered “flat”. In this frequency range two components pass with highly correlated gain and linear phase. The channel affects quite differently two sinusoids with frequency separation greater than B_C . If the coherence bandwidth is defined as the frequency interval over which the autocorrelation of the

channel's complex frequency transfer function is above 0.9, then the coherence bandwidth is approximated by [A.1]:

$$B_C \approx \frac{1}{50\sigma_\tau} \quad (\text{A.4})$$

Most commonly, the coherence bandwidth is defined as the bandwidth over which the value of the correlation function is at least 0.5. In this case we have [A.1]:

$$B_C \approx \frac{1}{5\sigma_\tau} \quad (\text{A.5})$$

An exact relationship between coherence bandwidth and rms delay spread does not exist.

Doppler spread and coherence time

While the delay spread and coherence bandwidth are parameters that describe the time dispersion nature in the channel due to its geometric and static characteristics, the *Doppler spread* and *coherence time* parameters describe the time varying nature of the channel in the small-scale region, caused by the relative movements between transmitter and receiver. To understand how Doppler spread can cause frequency dispersion at the receiver, we analyze how a channel behaves when a pure sinusoidal at frequency f_c is transmitted.

The received signal has spectral components in the range $f_c + f_D$ to $f_c - f_D$, where f_D is the Doppler shift.

The coherence time T_C is the time domain dual of the Doppler spread; it is a measure of the time during which the channel can be assumed as non-variant. In the Clark model [3.4], Doppler spread and coherence time are defined as being inversely proportional each other:

$$T_C = \frac{1}{f_{\max}} \quad (\text{A.6})$$

where f_{\max} is the maximum Doppler shift, defined in (2). Using a different model, in [A.10] the coherence time is defined as the time over which the value of the autocorrelation of the transfer function is above 0.5; then the coherence time is approximately defined as

$$T_C \approx \frac{9}{16\pi f_{\max}} \quad (\text{A.7})$$